A Rapid Method for Measuring Local Groundwater-Surface Water Interactions and Identifying Potential Non-Point Source Pollution Inputs to Rivers

A thesis submitted in partial satisfaction of the requirements for the degree

Master of Science in Environmental Systems

UNIVERSITY OF CALIFORNIA

Merced

by

Christopher Aaron Butler

May, 2009

Table of Contents

List of Figures

ABSTRACT OF THE THESIS

A Rapid Method for Measuring Local Groundwater-Surface Water Interactions and

Identifying Potential Non-Point Source Pollution Inputs to Rivers

by

Christopher A. Butler

Master of Science in Environmental Systems

University of California, Merced, 2009

Agriculture in the Central Valley of California is a potential contributor of non-point source pollution to surface waters via the groundwater pathway. This work presents a relatively simple method and inexpensive apparatus for quantifying local groundwater discharge into rivers using heat as a tracer. Two transects along a known gaining reach of the Lower Merced River were used to evaluate the effectiveness of the groundwater discharge monitoring instruments, known as Temperature Javelins, over three months. In terms of fulfilling deployment objectives, Temperature Javelins proved to be low cost, easy to install, and yielded easily interpretable data related to groundwater-surface water discharges. Groundwater discharge velocities were found to vary over time seasonally and spatially (on a scale of meters). Discharges ranged from 0.1 to 6.8 cm/day with higher discharge velocities found on the northern side of the river. These values are consistent with previous values obtained at the same site using other methods. Corresponding hyporheic water samples were collected to investigate solute transport (specifically nitrate) by the discharging water. Nitrate concentrations ranged from non-detectable to 50 ppm in these samples, where elevated values appear to be associated with groundwater entering on the north side of the river. Elevated nitrate flow lines in the hyporheic zone correspond with high discharge areas and alternate with ammonium enriched columns and low groundwater discharge. It is hypothesized that nitrification cells are induced by groundwater-surface water interactions. Testing of this hypothesis is proposed as a subject of further research.

Acknowledgements

This work was supported by the Center for Embedded Network Sensing (CENS) through the use of the National Science Foundation (Cooperative Agreement #CCR-0120778). In addition, the USGS's installation of infrastructure and extensive prior work on the study site for this research is gratefully acknowledged. Special thanks are extended to the Harmon research group of the University of California, Merced whose support in deployments and intellectual contributions to this work were vital to its success, and to my thesis committee for their thoughtful comments which vastly improved the quality of this document. The opinions, conclusions or findings of this work do not represent those of the supporting agencies.

Chapter 1 Introduction and Background

1.1 Introduction

The use of heat as a tracer to monitor the movement of groundwater was first documented by Suzuki (1960). Current methods for measuring subsurface temperatures within riverbeds can be discussed in terms of three categories. The first method involves the installation of temperature sensors in ephemeral streambeds when dry (Ronan et al., 1998; Stonestrom and Constantz, 2003). In a second approach, shallow temperature-recording piezometers can be inserted into a riverbed (Conant, 2004; Domagalski et al., 2007; Essaid et al., 2008; Stonestrom and Constantz, 2003; Zamora, 2007). The third method is to map the streambed temperatures by inserting a rigid temperature probe at a depth below the influence of the diurnal fluctuations of the surface water (Conant, 2004; Schmidt et al., 2007).

Problems and limitations are inherent with each method. The first method is only viable for ephemeral streams when dry, is labor intensive, and is limited to river reaches that are easily accessible. The second method relies on measuring the water temperature inside the piezometer, not the streambed sediments. Monitoring the water inside the piezometer allows for vertical flow of water within the piezometer and thus less accurate temperature measurements at depth. The third method may be not effective where there are low groundwater-surface water (gw-sw) exchanges and the riverbed is subject to diurnal influences at depths below 1 meter (m).

The objective of this work is to develop a low-cost method for logging vertical temperature profiles in saturated riverbed sediments. The method should be viable under both wet and dry stream conditions, and sensitive to the influence of diurnal fluctuations in the surface water temperature. The Temperature Javelin developed herein provides a straightforward method for obtaining streambed temperature profiles, which can then be interpreted to yield gw-sw discharges. This method has the potential for identifying sensitive river reaches which in turn may be linked to potentially problematic land management practices adjacent to the river.

The following chapters focus on the use of heat as a tracer, the proposed method, and the validation of this method. The remainder of this chapter focuses on the study site used for testing the Temperature Javelins, including a summary of the results from prior investigations at this location and concludes with a brief discussion of hyporheic flow exchanges in the context of biogeochemical processes that occur at the gw-sw interface within agricultural catchments. Chapter 2 contains a description of the theoretical underpinnings associated with the use of heat as a tracer as well as the effects of heat on substrate properties. Chapter 3 describes the fabrication and testing of the Temperature Javelin and the location and timing of the water quality sampling which coincided with the javelin testing. Chapter 4 presents the results and discussion emanating from this work. Chapter 5 contains a summary of the key conclusions from this investigation and discusses the future directions of this work, including the integration of water sample collection devices into a single unit with the temperature monitoring equipment.

1.2 Background

1.2.1 Study Site

As the Merced River extends from its source in the Sierra Nevada, through the San Joaquin Valley, to its confluence with the San Joaquin River, it passes through large expanses of agricultural and urban land. The study site for this work is located on a reach of the Lower Merced River, downstream of major impoundments. Agricultural land uses in this region include orchards, row crops, vineyards and dairies. It follows that the Merced River is impacted by agricultural practices in terms of point and non-point source pollution via both groundwater and surface water pathways. This work focuses on non-point source pollutant discharges to the river via the groundwater pathway.

1.2.2 Hydrogeology and Climate

The Lower Merced River Basin covers 831 km^2 (321 mi^2) and is underlain by a primary unconfined aquifer composed of alluvial deposits from the Sierra Nevada to the east and the Costal Ranges to the west (Gronberg and Kratzer, 2006). The map in **Figure 1.1** shows the location of the study site within the basin. Sediments tend to be coarse to fine-grained sands to a depth of approximately 40 m where the Corcoran Clay confining layer begins (Burow et al., 2004; Gronberg and Kratzer, 2006). The uppermost, unconfined aquifer follows the local topography with the water table measuring at a depth between 5.5 to 6.1m below grade, but varying with short-term climactic conditions and irrigation practices. Groundwater temperature remains relatively constant at 19.5 ˚C.

Climate at the site is characteristic of that of the central San Joaquin Valley, that is, arid to semiarid and can be distinguished as having hot summers and mild winters. Temperatures range from below 0°C to above 38°C (mid 30's to excess of 100°F)(Gronberg and Kratzer, 2006). Annual precipitation from 1931 to 1997 was 315 mm (Phillips et al., 2007), with 80% falling between November and March (Gronberg and Kratzer, 2006).

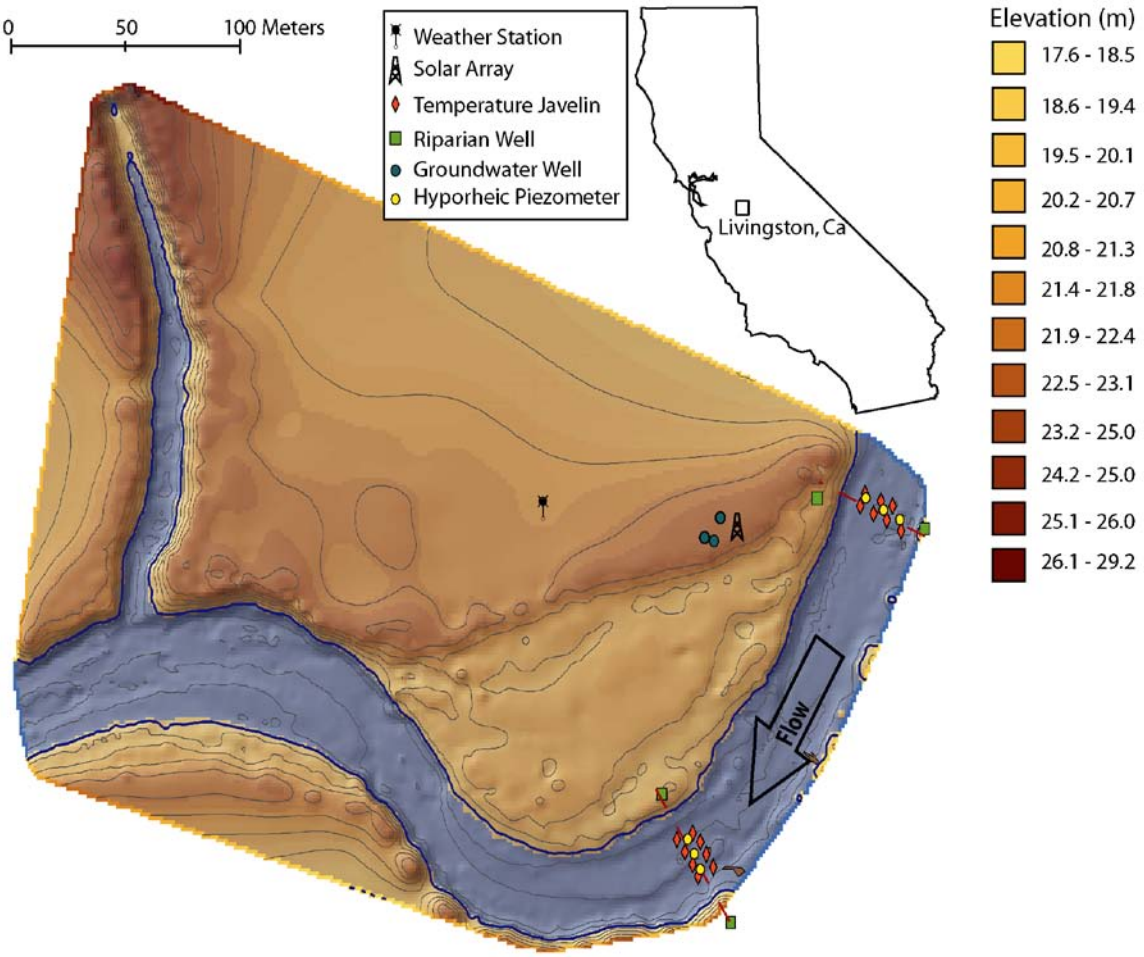

Figure 1.1 - Local site map near Livingston, Ca. highlighting current hydrologic monitoring infrastructure.

1.2.2.1 Lower Merced River

The Lower Merced River extends approximately 95 kilometers (59 miles)from Lake McClure to its confluence with the San Joaquin River at the west side of the San Joaquin Valley. The streambed is composed of gravel and coarse sand alluvial deposits. Historic median flows taken at the Merced River gauge near Stevenson (MST) is 7.0 m^3/s (248 cfs), ranging from 0.87 m^3/s (31 cfs) to35.8 m^3/s (1264 cfs) taken from 1999 to 2008 (**Figure 1.2**). Flows during the current investigation ranged from 7.8 m^3/s (203 cfs) to 12.2 m^3/s (432 cfs) with a median value of 8.3 m^3/s (291 cfs).

The Lower Merced River is managed for flood control, environmental sustainability and irrigation supply via releases from New Exchequer Dam upstream. The lower river is heavily managed for water supply and flood control. **Figure 1.2** shows the hydrograph of the Merced River over the past 10 years. Typical water years (e.g., 2001 to 2003) are characterized by spring and fall (usually May and November) releases mandated for protections of juvenile Chinook salmon migrating from the San Joaquin River to the Sacramento Delta as part of the Vernalis Adaptive Management Program (VAMP). Flows near 40 m^3/s (1400 cfs) are released in the

spring and near 20 m^3/s (700 cfs) in the fall (**Figure 1.2**). Selected spring VAMP flows are highlighted to differentiate the magnitude of flow releases compared to flows during other times of the year. Large water years are shaded to illustrate the high interannual variability of flows when flood control drives management decisions.

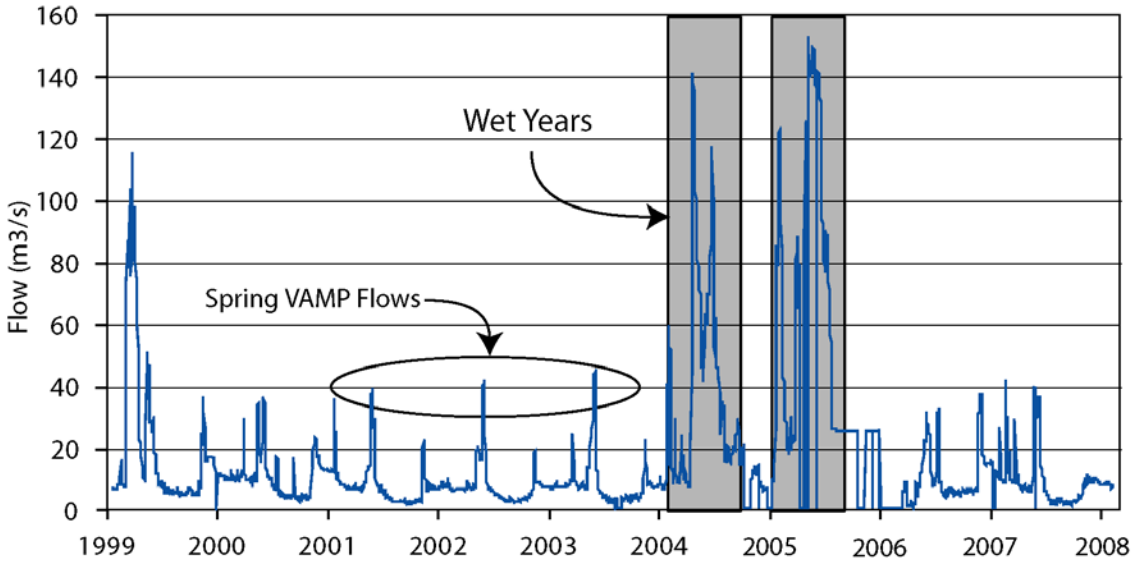

Figure 1.2 - Merced River hydrograph (1999 to 2008) (CDEC, MST Gauge station).

1.2.2.2 Land Use

Land use along the Lower Merced River encompasses urban and suburban areas, rangeland, livestock production facilities (e.g., chicken), dairies, and a variety of agriculture. Agricultural lands consisting of dairies, feed crops, orchards, and vineyards border approximately 65% of its length (Vogelmann et al., 2001). Most of the agricultural land is irrigated by surface water originating from the Merced River. Total Nitrogen (N) use in 2004 was approximately 7300 Mg (Gronberg and Kratzer, 2006). Three land use types dominate at the research site; almond orchards to the far north, row crops approaching the river, riparian vegetation bordering the Merced River, with vineyards to the south of the River (**Figure 1.3**).The nearby orchards are irrigated using sprinklers, row crops, such as corn, are flood-irrigated, and vineyards are predominantly irrigated using drip and sprinkler irrigation.

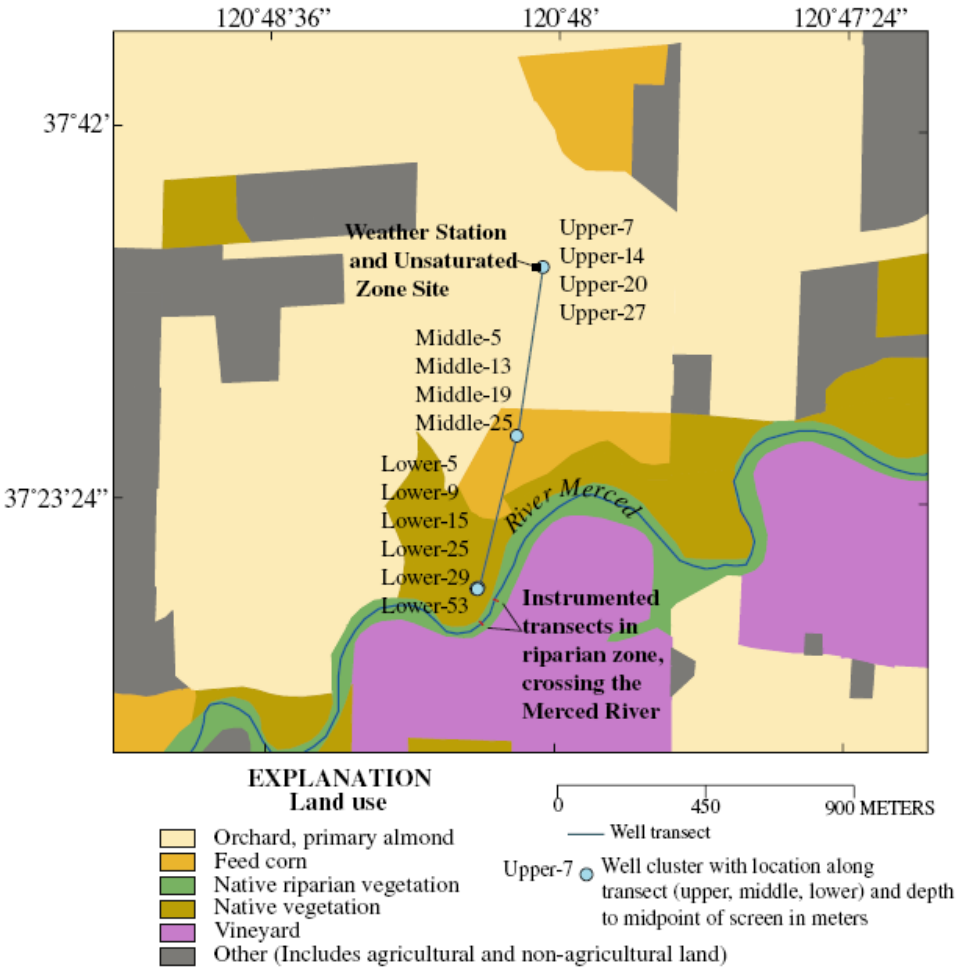

Figure 1.3 - Site map showing land use types and groundwater well transect nest depths and river transects (Domagalski et al., 2007).

1.2.2.3 Previous Site Investigations

As part of the National Agricultural Water Quality Assessment (NAWQA) program by the U. S. Geological Survey (USGS), many investigations have taken place at this location to determine agricultural impacts on the environment, as well as hydrologic behavior (Domagalski et al., 2008; Domagalski et al., 2007; Essaid et al., 2008; Fisher and Healy, 2008; Green et al., 2008a; Green et al., 2008b; Hancock et al., 2008; Phillips et al., 2007; Puckett et al., 2008; Steele et al., 2008; Vogel et al., 2008; Zamora, 2007). This body of work includes the development and testing of a regional and local multiscale groundwater model for tracking movement through the unsaturated and saturated zone (Phillips et al., 2007). The USGS group has traced nitrate from fertilizer applied to the orchard and row crops to the Merced River and identified denitrifying conditions at shallow depths in the aquifer and streambed (Domagalski et al., 2007). Zamora (2007) estimated groundwater discharge by comparing seepage meters, hyporheic piezometers to measure pressure head, and using heat as a tracer. This effort also concluded that seepage meters were unreliable for determining gw-sw discharges in the sandy substrate, whereas, using heat as a tracer was proved to be a viable method. Groundwater discharge velocities were found to be between 0.4 and 2.2 cm/d in this gaining reach (Zamora, 2007).

A comparison of multiple agricultural watersheds was published in a special issue of the *Journal of Environmental Quality* that included the site associated with this work (Capel et al., 2008; Domagalski et al., 2008; Essaid et al., 2008; Fisher and Healy, 2008; Green et al., 2008a; Green et al., 2008b; Hancock et al., 2008; Puckett et al., 2008; Steele et al., 2008; Vogel et al., 2008). Puckett (2008) determined that denitrification occurred in pockets within the hyporheic zone where there were elevated levels of dissolved organic carbon (DOC). In addition, Pucket (2008) observed surface water mixing to one meter below the streambed resulting in significant spatial variation in nitrate concentrations (Puckett et al., 2008). Essaid (2008) reported groundwater discharge velocities between -1.82 and 4.8 cm/day. This report also suggested that high flow releases trigger flow reversals from groundwater discharge to recharge. In addition, high flows purge the streambed of fine-grained materials, leading to rate changes in discharge due to alterations in local hydraulic conductivity. An additional conclusion of this work was that hyporheic flows at the site are more accurately described as multidimensional as opposed to the one-dimensional flow that many models assume (Essaid et al., 2008).

The Lower Merced River provides excellent opportunities to evaluate the effectiveness of Temperature Javelins in an agricultural basin. The study site retains the geologic, hydrologic, and climate found in the central San Joaquin Valley, and is characterized by a wealth of prior investigations carried out that are ideal for comparison with the current work.

Chapter 2 Heat Transfer in Subsurface Hydrology

2.1 Heat as a Tracer

Temperature has long been used as a tool to trace the movement of groundwater through the subsurface media and estimate its hydraulic parameters (Slichter, 1905; Stallman, 1963; White et al., 1987). Using a theoretical basis for the propagation of heat through groundwater, these researchers have provided analytical and numerical solutions to the differential equations describing heat transport through the subsurface media. Due to the difficulty observing groundwater behavior, the use of this property can be used in conjunction with other methods to better estimate hydrologic parameters of the subsurface medium (Anderson, 2005; Lapham, 1989; Stonestrom and Constantz, 2003).

Heat transfer through groundwater is a result of two main processes, conduction and convection. Conduction is the transfer of heat from areas of high to low temperatures due to a thermal gradient, and is independent of flow. It can be the dominant heat transfer mechanism in slow-moving groundwater. The pressure-driven process of heat transfer is referred to as forced convection. Relatively large temperature gradients can lead to density differences causing buoyancy-driven flow, known as free convection, but this requires relatively large temperature differences.

Conductive heat transfer as a one-dimensional flux (J_x) is described by Fourier's Law:

$$J_x = -K_T \frac{dT}{dx} \tag{1}$$

where, K_T is the thermal conductivity of the solid-fluid matrix, and $\frac{dT}{dx}$ is the temperature gradient in the x direction. The convection-conduction model considers both the conductive and convective modes of heat transfer (Stallman, 1965):

$$\frac{K_T}{\rho c}\nabla^2 \mathrm{T} - \frac{\rho_f c_f}{\rho c}\nabla \cdot (Tq) = \frac{\partial T}{\partial t} \tag{2}$$

Where, T (K) is temperature, z (m) is the depth below the streambed, K_T ($W \cdot m^{-1}K^{-1}$) is the thermal conductivity of the solid-fluid matrix, t (s) is time, q_z ($m \cdot s^{-1}$) is fluid velocity, $\rho_f c_f$ ($J \cdot m^{-3}K^{-1}$) and ρc ($J \cdot m^{-3}K^{-1}$) are the volumetric specific heat of the fluid and solid-fluid matrix respectively, where ρ ($kg \cdot m^{-1}$) and c ($J \cdot kg^{-1}K^{-1}$) are the corresponding density and heat capacities. Equation 2 describes both the advective and conductive forces in the groundwater. The first term in (2) describes the conductive or diffusive forces involved in the transport of heat in groundwater. The second term in (2) describes the advective or convective forces.

2.2 Thermal Effects on Hydraulic Conductivity

Changes in surface water temperature are known to influence the rate at which discharge into rivers by changing local hydraulic conductivity values (Anderson, 2005; Constantz, 1998; Constantz and Thomas, 1997; Constantz et al., 1994; Rorabaugh, 1956; Winslow, 1962). Hydraulic conductivity is inversely proportional to the dynamic viscosity of water (μ_w) and directly proportional to density, which are both influenced by temperature:

$$K_H = \frac{kg\rho_w}{\mu_w} \tag{3}$$

where, k is intrinsic permeability, g is gravity, and ρ_w is the density of water. As the streambed temperature increases, for example, within a normal range, the viscosity of water decreases, increasing the hydraulic conductivity and allowing greater discharge into the surface water for the same pressure gradient. Constantz (1994) reports up to 30% greater groundwater discharge during the afternoon compared to morning from the change in hydraulic conductivity of temperature (Constantz et al., 1994). The density of water also decreases with increasing temperature, albeit modestly over the range of temperatures observed at this site, resulting in enhanced hydraulic conductivity.

2.3 Thermal Signal in Groundwater Movement

Early successes in the use of heat as a tracer set the stage for widespread use of the temperature to monitor the movement of groundwater (Bredehoeft and Papadopulos, 1965; Domenico and Schwartz, 1990; Stallman, 1963; Suzuki, 1960). More recent work has demonstrated that tracking heat transfer is a highly effective method for estimating groundwater flow and hydraulic properties in porous media (Conant, 2004; Constantz et al., 2001; Constantz and Thomas, 1997; Essaid et al., 2008; Johnson et al., 2005; Schmidt et al., 2007; Stonestrom and Constantz, 2003).

Bredehoef (1965) was one of the first to develop an analytical solution (4) to Stallman's (1965) equation (2) and developed a type curve method for estimating groundwater velocities based on temperature measurements:

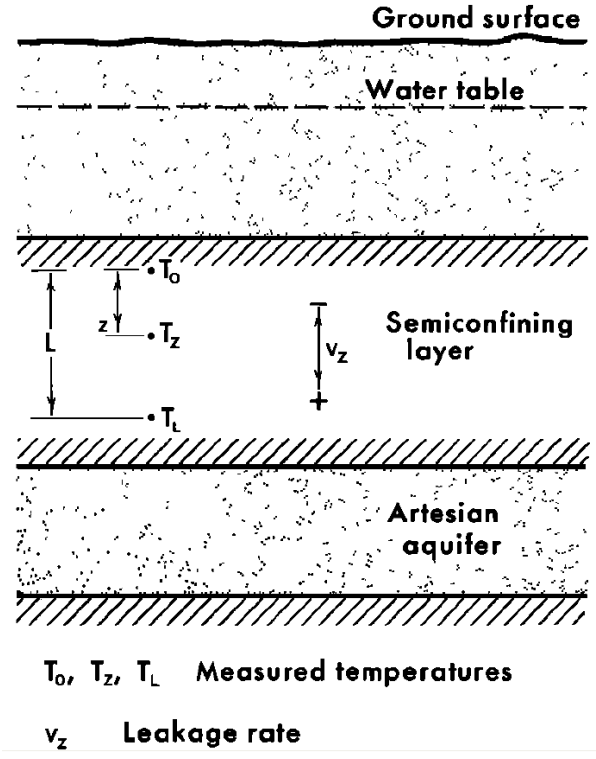

Figure 2.1 - Diagrammatic sketch of typical leaky aquifer (from (Bredehoeft and Papadopulos, 1965) ©Amer. Geophys. Union).

$$T_z = T_0 + [T_L - T_0]\frac{\left[exp\left(N_{P_e}\frac{z}{L}\right)-1\right]}{\left[exp\left(N_{P_e}\right)-1\right]} \quad (4)$$

where T_0 is the temperature at the upper most boundary at z =0, T_L is the temperature at the lowest measurement at z = L, T_z is the temperature at any depth over the thickness L. N_{Pe} is the Peclet number for heat transfer and is defined in (5).

$$N_{P_e} = \frac{\rho_w c_w q_z L}{K_T} \quad (5)$$

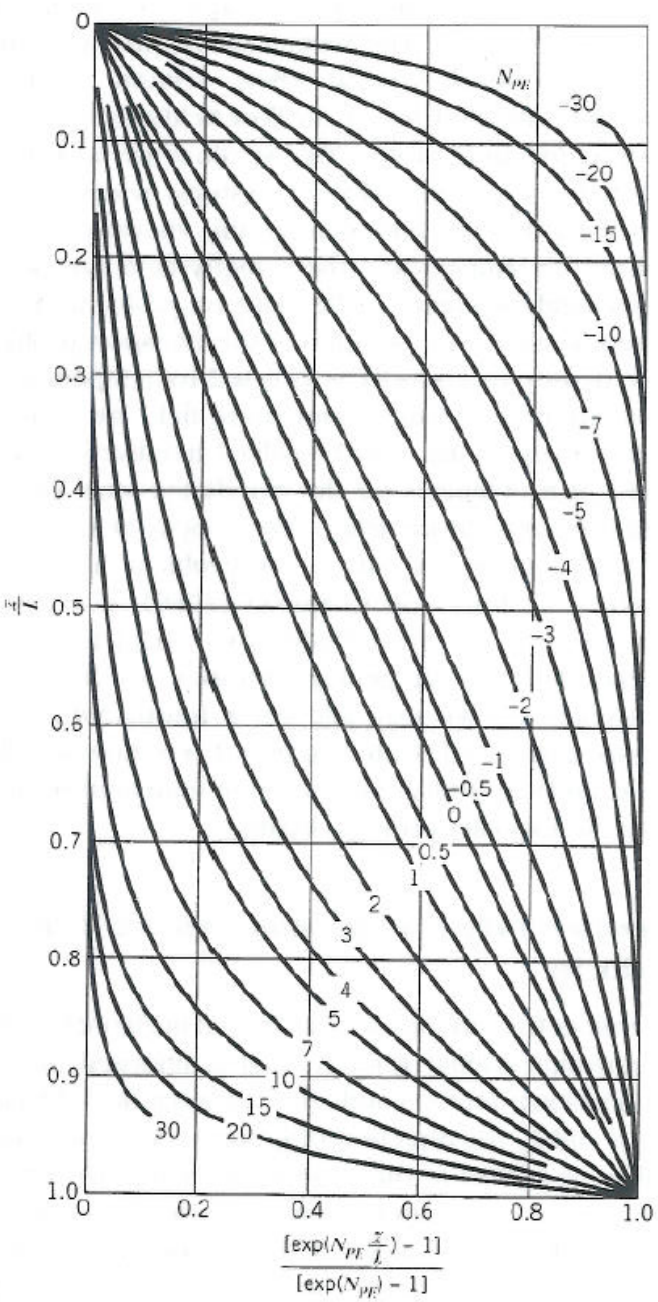

Figure 2.2 – Type curves for solution of one-dimensional conduction-convection equation (modified from(Bredehoeft and Papadopulos, 1965) ©Amer. Geophys. Union).

Figure 2.2 represents an analytical solution to (2) in terms of Peclet numbers as a function of a normalized streambed temperature $(T_z - T_0)/(T_L - T_0)$ for a depth factor (z/L) (Domenico and Schwartz, 1990). The velocity can be derived from (5) after field plots are determined. Bredehoeft and Papadopulos (1965) suggested that a minimum detectable groundwater velocity is a function of the thermal conductivity, volumetric heat capacity of the solid-fluid matrix, and the length over the measurements (6).

$$|q_z| = \frac{0.5K_T}{\rho_f c_f L} \quad (6)$$

Stonestrom and Constantz (2003) present the basic theory of the use of heat as a tracer (**Figure 2.3**), methods for using heat as a tracer in the monitoring of gw-sw exchanges, as well as multiple studies. **Figure 2.3** describes the theoretical conditions of gaining and losing reaches within a stream. Slide (A) shows an increase in head from within the streambed compared to the surface water, as well as a muted diurnal temperature influence with depth. Slide (B) depicts a decrease in head within the streambed compared with the surface water, and a much greater influence of the diurnal temperature fluctuations of the surface water within the streambed as it recharges the hyporheic zone(Stonestrom and Constantz, 2003).

Stonestrom and Constantz (2003) present 7 cases illustrating the use of heat to investigate gw-sw interactions. Rillito Creek near Tucson Arizona, the Rio Grande in New Mexico, the Willamette Basin in Oregon, and the Trout Creek in Nevada investigations were supported by numerical infiltration models to determine infiltration rates from the surface water to the groundwater for future water planning, irrigation pumping effects on the groundwater flows and to quantify the amount of seepage loss from snowmelt respectively. The Russian River in Northern California, Santa Clara River in Southern California, Troute Creek near Lake Tahoe, California were investigated to understand gw-sw interactions in order to better track nutrient and chemical exchanges(Stonestrom and Constantz, 2003).

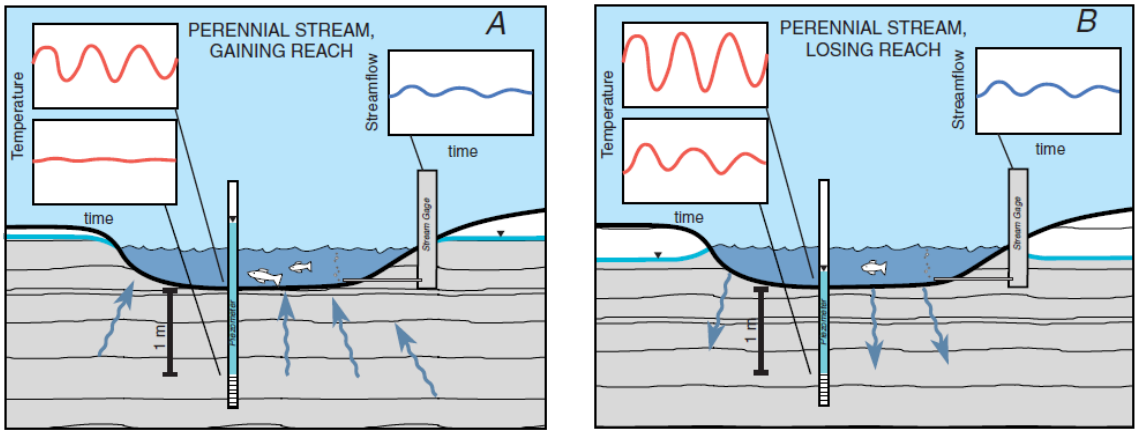

Figure 2.3 - Theoretical cross sections of gaining (A) and losing (B) streams (Stonestrom and Constantz, 2003).

Using empirical relationships between streambed temperatures and a Darcy flux, Conant (2004) modeled an ephemeral stream under quasi-steady-state conditions as a proxy for groundwater recharge rates. Streambed temperatures were obtained twice a year by inserting a temperature probe at a 0.2 meter depth, below the influence of diurnal temperature variations, every 1 meter along transects with a 2 meter spacing between transects. Darcy fluxes were estimated by performing slug tests on 34 mini-piezometers distributed to cover a range of streambed temperatures. Correlations were determined between the streambed temperature, and Darcy's law flux results. Correlations were reasonable (R^2=0.66 during summer mapping and R^2= 0.81 during winter mapping), and Conant found that this temperature method estimated groundwater fluxes reasonably well under most conditions. However, relationships were found to fail once streambed temperatures approached either groundwater or surface water temperatures (Conant, 2004; Schmidt et al., 2007).

In a recent investigation, Schmidt (2007) compared the Conant (2004) streambed mapping method with the USGS VS2DH transient model and an analytical steady state groundwater-surface model (Turcotte and Schubert, 1982)

$$q_z = \frac{K_T}{\rho_f c_f \cdot z} ln \frac{T(z) - T_L}{T_0 - T_L} \quad (7)$$

Schmidt (2007) found that analytically modeled fluxes validated the previous fluxes derived from empirical streambed measurements. In addition Schmidt (2007) found the steady-state analytical method proved to be accurate with less data than are required by numerical models (Schmidt et al., 2007).

Essaid (2007) characterized gw-sw interactions in five watersheds, including that associated with the site of this investigation, to compare gw-sw interactions across the sites using heat as a tracer. This researcher observed small groundwater discharge flows with flow reversals occuring during high stream flows(**Figure 2.4**)(Essaid et al., 2008). Groundwater discharge was found to increase during winter months, and reverse (becoming groundwater recharge) in response to high flows large releases by the upstream dam. Model (VS2SH) results agreed with observed streambed fluxes, and were validated using streambed seapage meters (Zamora, 2007), with streambed velocities ranging from -0.95 to 5.1 (cm/day) with a mean value of 1.1cm/day (Essaid et al., 2008).

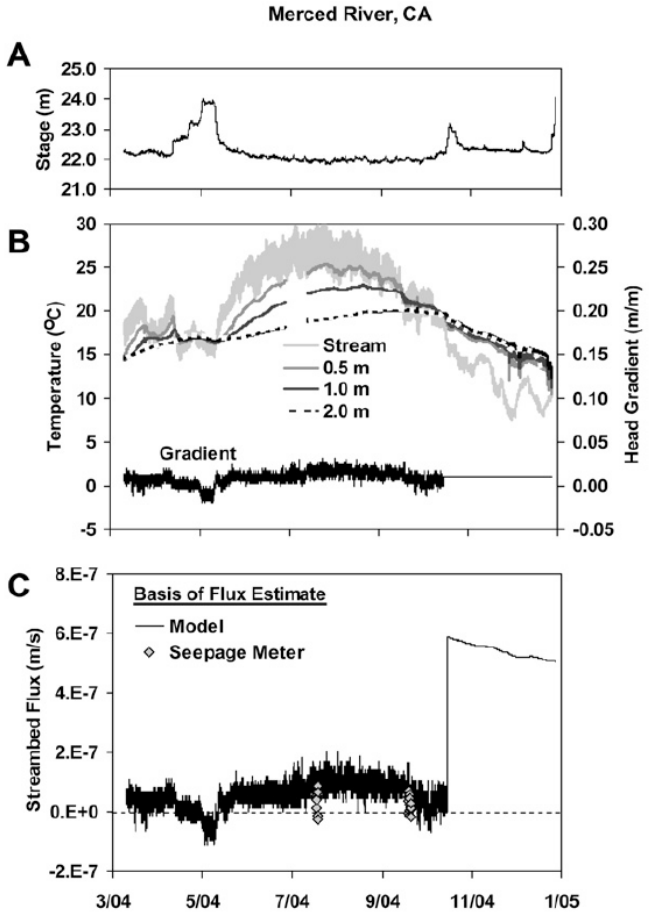

Figure 2.4 - Observed plots (A)stream stage, (B) temperature and head, (C) estimated streambed flux (Essaid et al., 2008).

In summary, the use of heat as a tracer has been found to be a valuable method to monitor the movement of groundwater (Anderson, 2005; Conant, 2004; Constantz, 1998; Essaid et al., 2008). Since its early discovery by Suzuki (1960) and Stallman (1960) many solutions have been developed to quantify the movement of groundwater through the subsurface as well as its interactions with the surface water.

Chapter 3 The Hyporheic Zone

The hyporheic zone is situated in streambed sediments where groundwater and surface water interface and mix (**Figure 3.1**). This zone is known to be a location of complex flow dynamics and high biogeochemical activity (Bencala, 1993; Bencala, 2000; Birgand et al., 2007). Mulholland and DeAngelis (2000) state that, "high ratios of surface area sediments to volume of water within sediments should result in large effects of microbial processes on subsurface water, and relatively slow advective flow of water within the subsurface zone retards the downstream movement of soluble materials compared with the surface environment." Both the flow reduction of and the biogeochemical reactions that take place in this zone are of great importance to the river ecosystem.

The study of hyporheic behavior is to a good measure still unknown and an active area of study (Bencala, 2005). Modeling of hyporheic flows continues to make progress using such models as One-dimensional Transport with Inflow and Storage (OTIS) and the Transient Storage Model (TSM). These models aid investigators in determining the residence time of hyporheic flows and thus their role in any different biogeochemical processes. The heterogeneity of the streambed sediments can greatly affect the hyporheic interactions spatially, even within the same reach (Salehin et al., 2004).

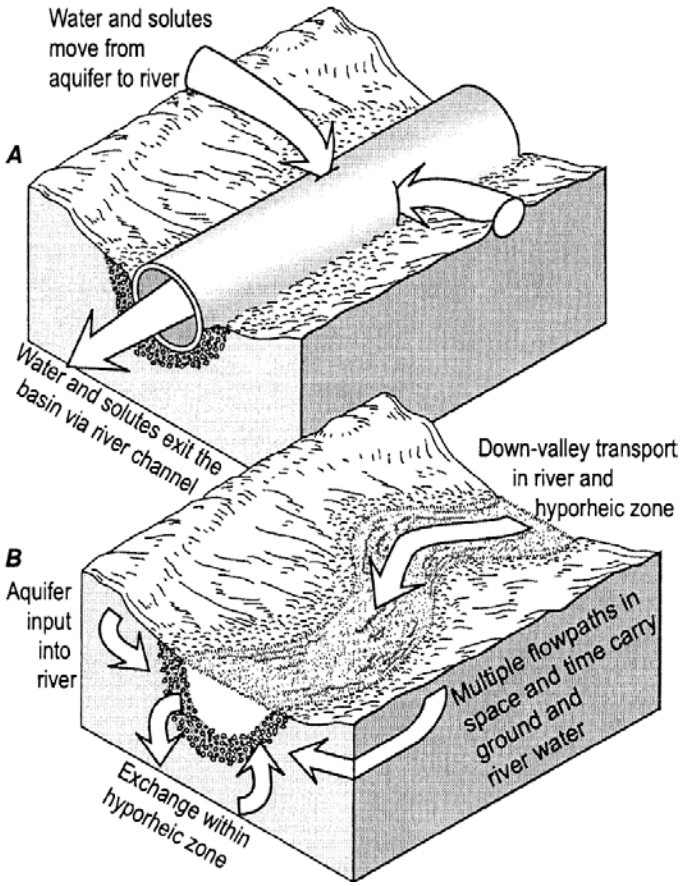

Figure 3.1 - (A.) Visualization of gw-sw interactions in a river system as a pipe; (B.) Alternate visualization of groundwater and surface water interacting within the river catchment (Bencala, 1993; Bencala, 2000).

Hyporheic flows are governed by the structure and hydraulic conductivity of the streambed alluvium or substrate, the hydraulic gradient locally across geomorphological features, and the presence or absence of groundwater fluxes entering the substrate (Storey et al., 2003). A key feature of hyporheic flow is to increase residence time of surface water coming in contact with biogeochemically active substrate for the transformation of solutes. It has been proposed that heterogeneous substrate deposits, and surface obstructions (Birgand et al., 2007; Cardenas and Zlotnik, 2003) play lesser roles in determining hyporheic flow dynamics. However, spatial variability of gw-sw hydraulic and biogeochemical interactions remains an area of active research.

A conceptual model for hyporheic zone flow is shown in **Figure 3.2**. Riverbeds are composed of a non-homogeneous mixture of porous alluvium. As water passes into the hyporheic zone, it moves out of the traditional stream channel, and into the banks and below the river itself. Partially submersed obstacles and debris induce areas of lower and higher pressure that also influence hyporheic flows (see 6, 7, and 11 in **Figure 3.2**). Here water travels below the riverbed and is drawn beneath an obstacle, and is "pumped" vertically on the lee side of the obstacle by a pressure decrease.

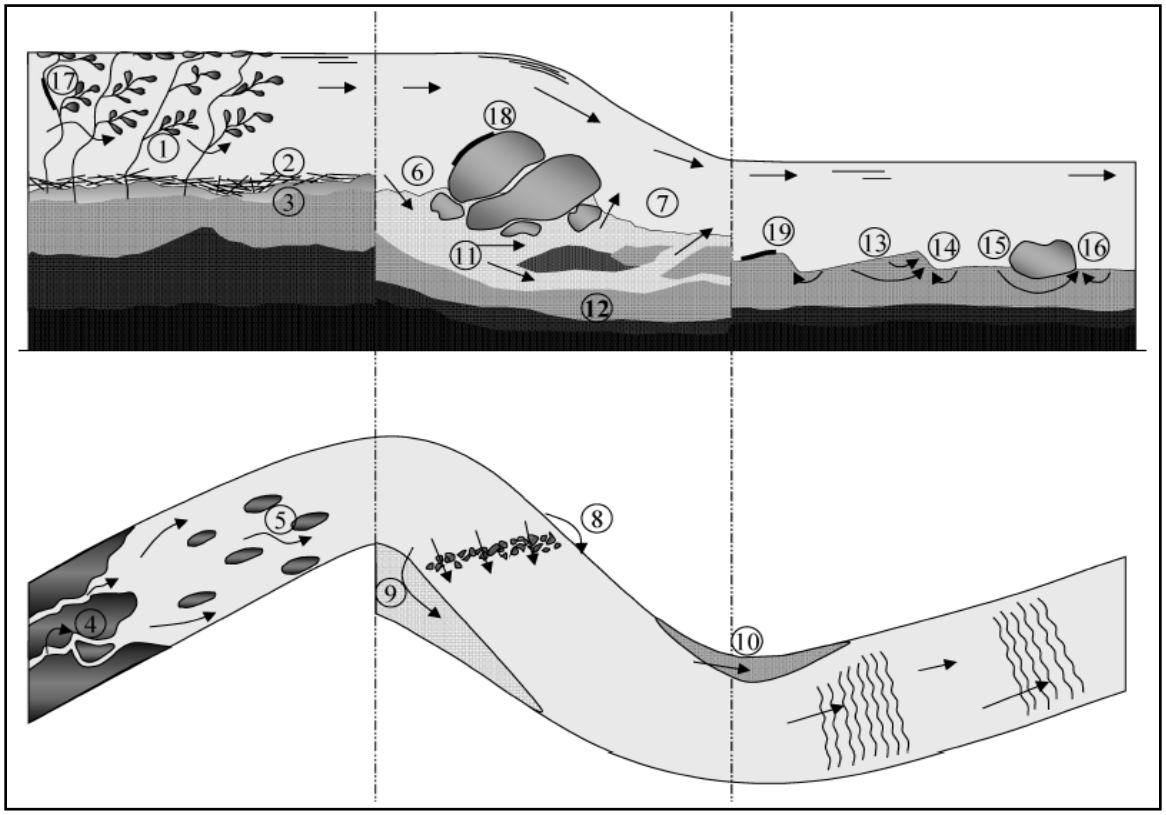

Figure 3.2 - Hyporheic flow dynamics and river solute interactions (Birgand et al., 2007).

3.1 Biogeochemical Reactions

When surface water breaches the surface water-riverbed interface and enters the hyporheic zone, it moves at a significantly slower rate, increasing its exposure to biogeochemically active substrate necessary for chemical transformations (Bencala, 2000; Birgand et al., 2007; Puckett et al., 2008). For example, denitrification is common, and there may a significant amount of nitrogen taken up by macrophytes and/or periphyton. Birgand (2007) suggests that between 350 and 1250 mg N/m^2 day is taken up by plants in agricultural catchments. Numerous studies have shown that in agricultural catchments, uptake by macrophytes and biofilms can be the dominant removal process of nitrate (Birgand et al., 2007). In each case unique plant physiology determines the activity site (e.g. roots, shoots, leaves) as well as rates of uptake.

Both laboratory and field studies have revealed various pathways of nitrogen uptake. Biofilms create anoxic areas within the film making denitrification possible, and reduce water velocities allowing longer residence times for nitrate in the water to be transformed (Nielsen and Sloth, 1994). Macrophytes, in addition to slowing surface water velocities (**Figure 3.2**), are able to change their uptake sites from shoots in the water column to their roots in the substrate, to better access nitrogen (Chambers et al., 1989; Cooper and Cooke, 1984; Vincent and Downes, 1980).

In summary, the hyporheic zone is a dynamic region where groundwater and surface water flow intermix and biogeochemical reactions are intricately intertwined to these flows. Hydraulic flows are unique to the reach scale of each river, with varying amount s of vertical and horizontal mixing. As a result biogeochemical reactions are equally heterogeneous. This method is uniquely well suited to aid in the understanding of this highly dynamic region surrounding rivers by decreasing the spatial scale which flow data can be collected.

Chapter 4 Materials and Methods

4.1 Site Infrastructure

As part of a the NAWQA program the USGS selected the Lower Merced River Basin to assess the fate and transport of agricultural chemicals moving along a groundwater flow path towards the Merced River (Phillips et al., 2007). The site was developed by the USGS with a groundwater well transect and two river transects to monitor gw-sw interaction. The groundwater transect is composed of three observation well nests positioned along a flow path extending from an orchard to the river over a distance of about one kilometer (**Figure 1.1**, **Figure 1.3**); the riparian zone is mapped below and includes the locations of nested observation wells at the foot of the groundwater transect as well as the riparian observation wells, and the new infrastructure stemming from the present research, the Temperature Javelins, which are described below (**Figure 4.1**,**Figure 4.2**). The river transects are spaced approximately 100 m apart and composed of two shallow riparian wells bounding each transect approximately 5 meters below grade and hyporheic transect piezometer pairs approximately 1.5 and 3 meters deep located along each side and middle of both transects. Water sampling drive points (**Figure 4.1**) correspond to hyporheic piezometers in each river transect. Additional site descriptions will follow in later sections.

4.2 Temperature Javelins

Temperature Javelins monitor streambed temperatures directly. Thermocron iButton self-logging thermisters (Model DS1922L, Dallas Semiconductors, Sunnyvale, CA, USA) were installed in 1.25 in. by 10 ft. (3.02 cm by 3.05 m) PVC pipe. Mounting holes were counter bored and tapped to allow set screws to secure the thermisters in the opposing sidewall (**Figure 4.2**). Custom machined drive tips capped on the bottom of the javelin.

Table 4.1 - Specified precision of monitoring equipment used to estimate groundwater discharge rates.

Model	Manufacturer	Operating Range	Precision	Measurement Type
Thermocron iButton DS1922L	Dallas Semiconductor	-40 to 85°C	0.5°C	Temperature
Model 101 (P2 stainless steel) water level meter	Solinst Canada Ltd.	0 to 30 m	0.005 m	Water Level
U20-001-01	Onset Computer Corporation	-20° to 50°C	±0.37°C at 20°C	Temperature
U20-001-01	Onset Computer Corporation	0 to 207 kPa	0.02 kPa	Pressure

Fifteen Temperature Javelins were installed in tandem transects along both hyporheic piezometer transects both upstream and downstream to bound the transect measurements. Javelins were driven into the streambed using a slide hammer every 5 m along a parallel transect that was 2 m offset from the hyporheic piezometer transect centerline (**Figure 4.1**). Temperature Javelins were inserted to depth, positioning the iButtons at the desired depths below the surface water-streambed interface (0.5, 1.0, and 2.0 m).

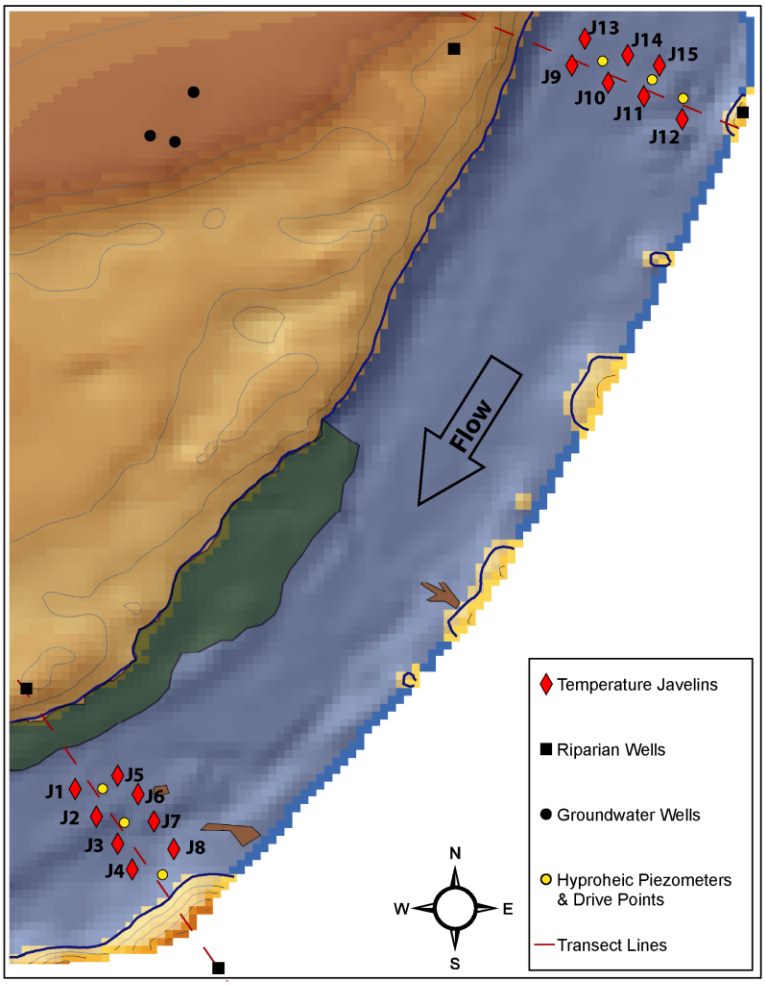

Figure 4.1 - Horizontal layout of the Temperature Javelins and hyporheic infrastructure.

Measurements were collected from October 16, 2008 through January 14, 2009. Streambed temperature measurements were monitored every 30 minutes using Temperature Javelins. Groundwater temperatures were measured at the local groundwater well cluster (**Figure 1.3**) at a depth of 40 m below grade using water level loggers (Model U20-001-01, Onset Computer Corporation, Pocasset, MA, USA) and found to be relatively constant. Surface water temperatures and stage were assumed to be identical to an upstream gauge station (MST), and thus MST gauge station data was used.

Hyporheic transects were instrumented by the USGS with water-sampling drive points at depths corresponding to the Temperature Javelins thermistor depths (0.5, 1.0, 2.0 m below the surface water-streambed interface). Drive points were installed at depth with sample tubing extending to the nearest bank at each hyporheic transect (Domagalski et al., 2007). Water samples were collected on October 16, December 10, and January 14, 2009 using a peristaltic pump (Model 401, Solinst Canada Ltd., Georgetown, Ontario, Canada), filtering (2.0µm filter), measuring electrical conductivity (EC) (Model EC300, YSI Inc., Yellow Springs, OH), and icing until analysis could be preformed. Water samples were analyzed using Ion Chromatography (IC) EPA method 800 for major ions.

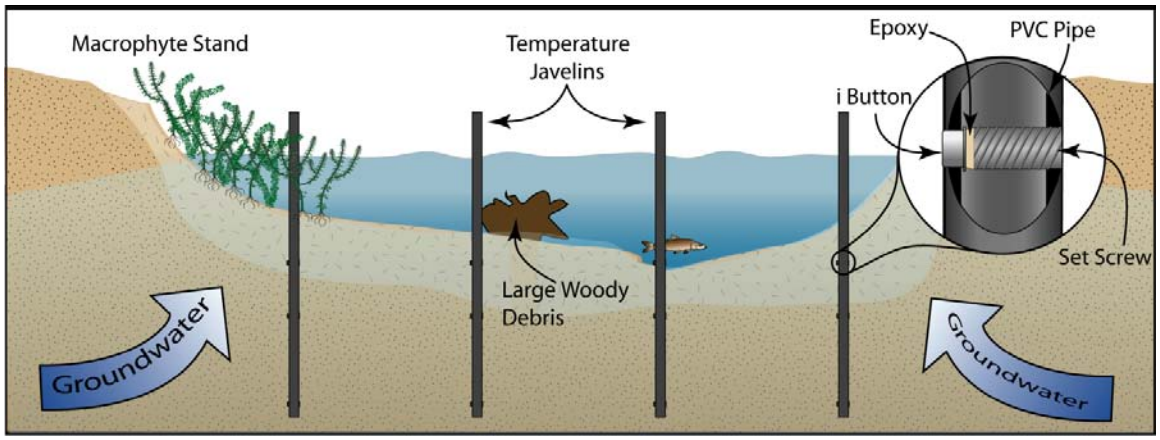

Figure 4.2 - Conceptual model and Temperature Javelin details and deployment positioning.

4.3 Analytical GW-SW Heat Transfer Model

Temperature Javelins yield vertical temperature distributions from which gw-sw discharge rates are calculated. Stallman (1965) used equation (2) to describe temperature redistribution as a function of heat transfer via convection (or advection) and conduction, an approach that has since lead to the development of several analytical models for gw-sw exchanges. This approach assumes that vertical temperature distributions in groundwater underlying a streambed are governed only by conductive and advective processes (i.e., no density driven flow), and that the porous media properties are homogeneous.

Various analytical solutions to (2) have been presented (Bredehoeft and Papadopulos, 1965; Stallman, 1965; Stonestrom and Constantz, 2003; Suzuki, 1960; Turcotte and Schubert, 1982) to the heat transport equation presented by Stallman (1965). This method utilizes one such analytical solution shown in equation (8) (Turcotte and Schubert, 1982) derived by assuming steady state upward vertical flow conditions and applying constant temperature boundary conditions at the streambed water interface (z=0, $T=T_0$), and deep in the river bed (as $z\rightarrow\infty$, $T=T_L$), where T_L is the deeper (constant) groundwater temperature. T(z) is the temperature at a given depth z, and T_0 is the temperature at the upper boundary; which in this case is the stream water temperature (see **Figure 4.3**).

$$\frac{T(z)-T_L}{T_0-T_L} = exp\left(-q_z \frac{\rho_f c_f}{K_T} z\right) \quad (8)$$

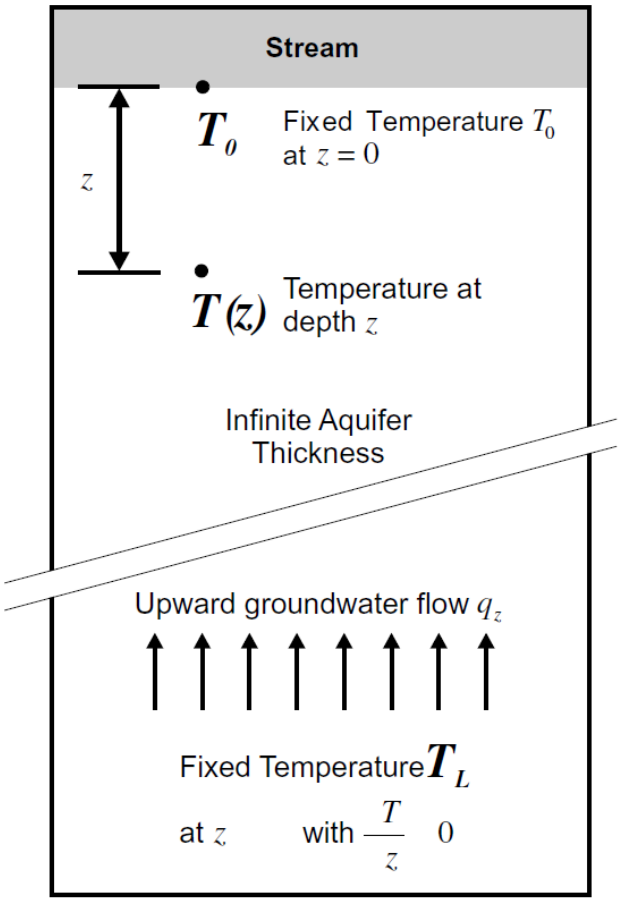

Figure 4.3 - Conceptual diagram of analytical solution by Turcotte and Schubert (1982) (drawn by Schmidt et al., 2007).

The steady state assumption is appropriate in many gw-sw systems, where pressure head differential (driving the discharge) and temperature distributions are not changing appreciably over time. If the system is in a period of significant flow change, as is common in many managed waterways, this assumption may not be appropriate. Equation (8) requires that the temperature difference between the groundwater and surface water be sufficiently great to cause a discernable vertical temperature gradient within the substrate. If the temperature difference is insufficient, then the uncertainty of the system will be too large to obtain reasonable parameter estimates, as will be demonstrated below (Bevington and Robinson, 1992).

Solving for the upward vertical groundwater discharge velocity, q_z yields the following form of the solution:

$$q_z = \frac{K_T}{\rho_f c_f \cdot z} ln \frac{T(z) - T_L}{T_0 - T_L} \qquad (9)$$

Assuming steady state conditions are well-approximated, temperature gradient data can be evaluated using (9) to yield an estimate of the vertical velocities at a given depth given reasonable estimates for the thermal conductivity value and the volumetric heat capacity for the solid-fluid matrix.

Figure 4.4 shows the analytical model behavior in the case where local groundwater is warmer than surface water (Turcotte and Schubert, 1982). For this calculation, groundwater is held constant at 19°C and surface water varies between 7°C and 15°C, which is consistent with the observed groundwater and surface water temperatures at t he current field site. The model calculates negative fluxes, or recharge when the streambed temperature (T_z) is less than the surface water temperature (T_0). Negative values in this model are invalid as it was derived to address gaining conditons only. While negative values obtained by this method could indicate actual recharge zones, the magnitude of the flux should be estimated using alternative models. Zero flux is observed when T_z is equal to T_0. Once T_z is greater than T_0, a positive velocity, or groundwater discharge is calculated. The model produces invalid results once T_z is equal or greater than the groundwater temperature (T_L) as it extends beyondthe model boundary conditions. Physically the model is constrained to operate successfully within a temperature envelope bounded by the groundwater and surface water temperatures.

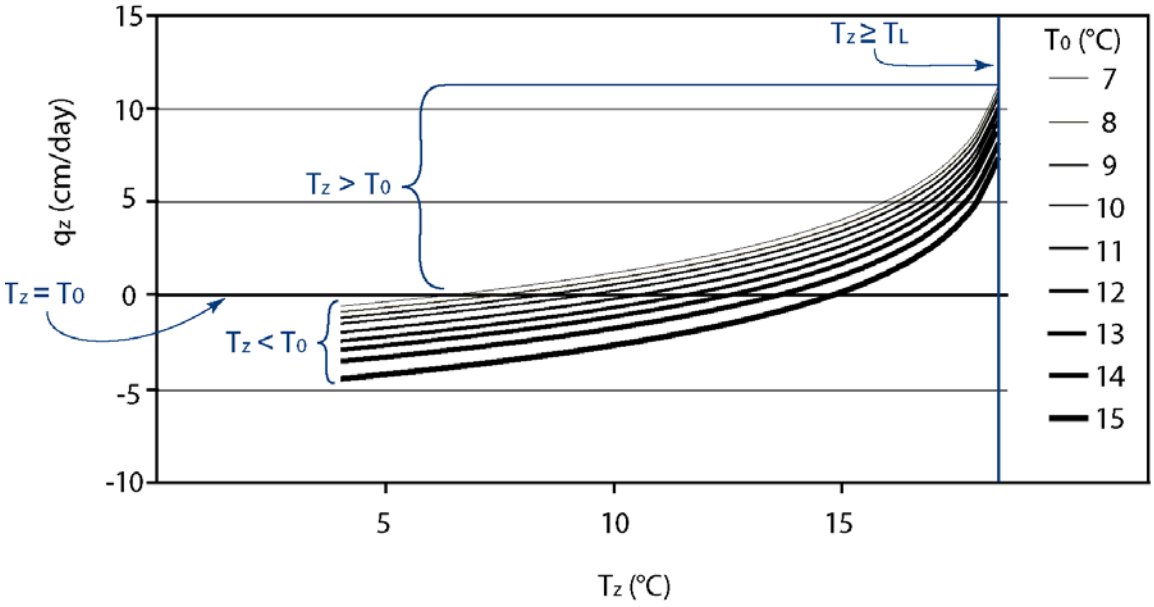

Figure 4.4 - Velocity changes with respect to streambed changes over variable surface water temperatures.

4.4 Estimating Groundwater-Surface Water Discharge Uncertainty

As each measurement or parameter estimation is made, there is uncertainty associated with it. These uncertainties propagate through the subsequent calculations to impart an aggregate uncertainty in the discharge estimate. Thus it is important to understand the uncertainties associated with each value and its effect on the overall output of the model (Bevington and Robinson, 1992). Through the use of the Gaussian error propagation method, the uncertainty associated with each parameter in the Turcotte and Schubert model can be estimated as indicated in (10), based on the partial derivatives of a variable ($\partial z/\partial x$), the uncertainty associated with the variable's measurement (σ_x), and the correlation of the dependent variables (σ_{xy}) (note: here x, y and z designate the variables illustrating the error

propagation method and are not to be confused with the coordinate system). This approach assumes that the errors associated with measurements and parameter estimates are known and normally distributed about the true value.

$$\sigma_z = \sqrt{\left(\frac{\partial z}{\partial x}\cdot\sigma_x\right)^2 + \left(\frac{\partial z}{\partial y}\cdot\sigma_y\right)^2 + 2\sigma_{xy}\cdot\left(\left(\frac{\partial z}{\partial x}\cdot\sigma_x\right) + \left(\frac{\partial z}{\partial y}\cdot\sigma_y\right)\right)} \quad (10)$$

Assuming independence between variables in (10) yields (11), where uncertainty in z (σ_z) is shown as square root of the sum of the squares of the partial derivatives of z with respect to each variable multiplied by the uncertainty for each variable.

$$\sigma_z = \sqrt{\left(\frac{\partial z}{\partial x}\cdot\sigma_x\right)^2 + \left(\frac{\partial z}{\partial y}\cdot\sigma_y\right)^2} \quad (11)$$

The partial derivatives for each parameter and variable in (10) are summarized below. Sources of uncertainty for (10) measurements (±sd) are given in **Table 4.2**.

$$\frac{\partial q_z}{\partial z} = \frac{K_T}{\rho_f c_f \cdot z^2} ln\frac{T(z)-T_L}{T_0-T_L} - \frac{K_T}{\rho_f c_f \cdot z}\cdot\frac{1}{T(z)-T_L}\cdot\frac{\partial T}{\partial z} \quad (12)$$

$$\frac{\partial q_z}{\partial K_T} = \frac{-1}{\rho_f c_f \cdot z} ln\frac{T(z)-T_L}{T_0-T_L} \quad (13)$$

$$\frac{\partial q_z}{\partial T(z)} = \frac{-K_T}{\rho_f c_f \cdot z}\cdot\frac{1}{T(z)-T_L} \quad (14)$$

$$\frac{\partial q_z}{\partial T_0} = \frac{-K_T}{\rho_f c_f \cdot z}\cdot\frac{1}{(T_0-T_L)} \quad (15)$$

$$\frac{\partial q_z}{\partial T_L} = \frac{-K_T}{\rho_f c_f \cdot z}\cdot\frac{T(z)-T_0}{(T(z)-T_L)(T_0-T_L)} \quad (16)$$

Table 4.2 - Standard error based on vendor-specified measurement precision and parameter estimation (for thermal conductivity)

Parameter/Variable	Best estimate	Precision	Source
z, depth below streambed	0.05 m	σ_z = ±0.02 m	Total Station survey
K_T, thermal conductivity	1.7 W·m^{-1}K^{-1}	σ_{K_T}= ±0.1 W·m^{-1}K^{-1}	Domagalski et al., 2007
T_0, surface water temperature	16.7 ℃	σ_{T0} = ±0.2℃	MST gauge station
T(z), streambed temperature at depth z	18.72 ℃	$\sigma_{T(z)}$ ±0.2℃	iButton DS1922L
T_L, groundwater temperature	20.6 ℃	σ_{T_L}= ±0.2℃	HOBO U20-001-01
$\rho_f c_f$, volumetric specific heat	4.19 x 10^{-6} W·s·m^{-3}·K^{-1}	??	Estimate??

Partial derivatives were evaluated using parameter values from a preliminary investigation of site materials, or gleaned from the literature. Inserting the partial derivatives and thermal values into (11), we arrive at the following equations for describing the uncertainty associated with the vertical velocity (q_z).

$$\sigma_{q_z} = \sqrt{\left(\frac{\partial q_z}{\partial z}\cdot\sigma_z\right)^2 + \left(\frac{\partial q_z}{\partial K_T}\cdot\sigma_{K_T}\right)^2 + \left(\frac{\partial q_z}{\partial T(z)}\cdot\sigma_{T(z)}\right)^2 + \left(\frac{\partial q_z}{\partial T_0}\cdot\sigma_{T_0}\right)^2 + \left(\frac{\partial q_z}{\partial T_L}\cdot\sigma_{T_L}\right)^2} \quad (17)$$

$$\sigma_{q_z} = \sqrt{(1.27x10^{-7})^2 + (1.2x10^{-7})^2 + (7.2x10^{-9})^2 + (3.6x10^{-9})^2 + (-6.8x10^{-8})^2} \quad (18)$$

The above equation demonstrates the individual constituents of the uncertainty equation; it is evident that the first two components, depth and thermal conductivity, are the main contributors to uncertainty. Depth measurements and thermal conductivity are at least on order of magnitude greater than the remaining variables in the equation.

Figure 4.5 and **Figure 4.6** show the two main influences of the uncertainty of a single parameter on the uncertainty of the vertical velocity. By varying the uncertainty of each variable, and plotting against the uncertainty of the vertical velocity, we can quantify the sensitivity of the groundwater discharge estimate to measurement uncertainties associated with these variables. Here the parameters are typical for the test site of this study. The plot in **Figure 4.5** demonstrates, for example, that a thermal conductivity uncertainty of 0.01 W·m^{-1}K^{-1}has a minor effect on the overall uncertainty of the vertical velocity, and that at a reasonably expected uncertainty of 0.1 W·m^{-1}K^{-1}, the corresponding uncertainty in vertical velocity is about 18 percent. However, greater uncertainties in this parameter would render the discharge estimate highly uncertain for the present case.

The plots in **Figure 4.6** demonstrate the effect of the uncertainty of depth measurements on the vertical velocity uncertainty. For example an uncertainty of 0.02 m increases the vertical velocity uncertainty of nearly 18 percent. A decrease to 0.01 m would have virtually no effect on the overall uncertainty.

For the conditions of the test site the results of the uncertainty analysis indicate that the main source of uncertainty for the Temperature Javelins is the thermal conductivity. Given the current uncertainty parameters, the resulting uncertainty of the vertical velocity is less than 20 percent.

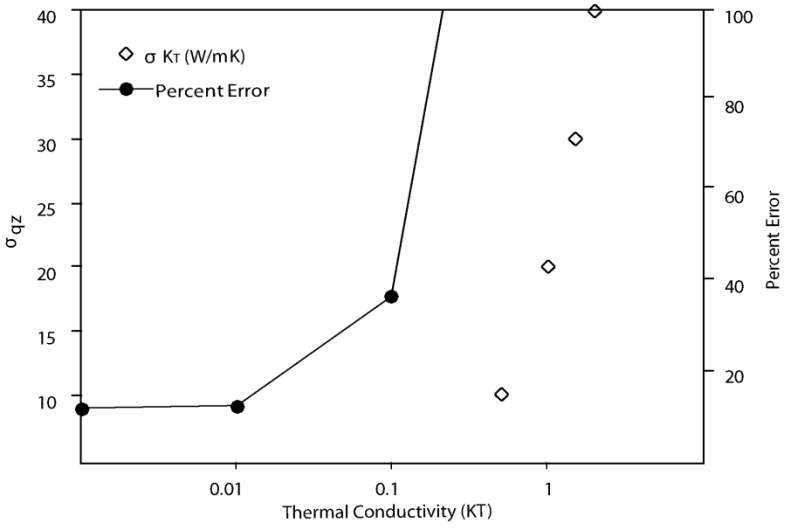

Figure 4.5 - Uncertainty in the estimated discharge value resulting from errors in the thermal conductivity parameter (Uncertainties of vertical velocities are shown in open circles; percent error is shown in connected black points).

Figure 4.6 - Uncertainty resulting from temperature depth measurements within the streambed.

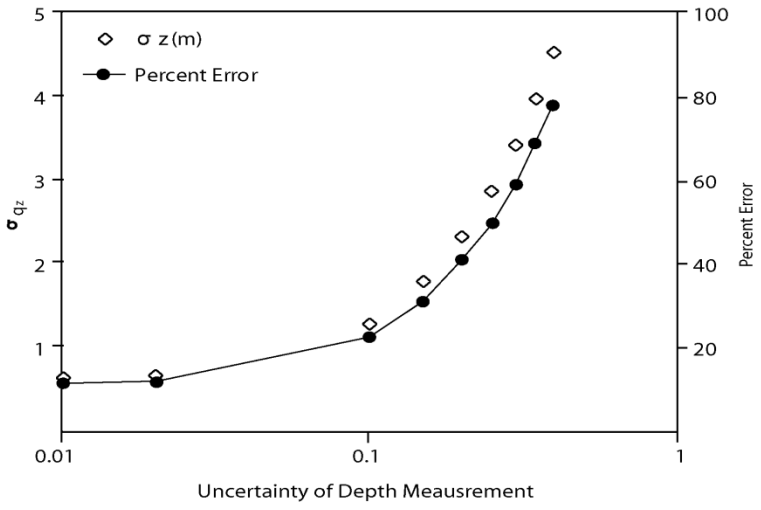

Using the above stated partial derivatives, parameter uncertainties, and values, model uncertainties can be obtained using (17). Model uncertainty given the stated values is 12 percent of the calculated vertical groundwater discharge velocity. This resulting uncertainty value associated with calculating groundwater discharge velocities using this model yields accurate results.

The previous chapter presents the development and deployment of the Temperature Javelins used to calculate groundwater discharge velocities. Temperature Javelins were constructed using inexpensive materials and deployed over a 3 month period. Groundwater discharge velocities were calculated using a one-dimensional analytical model. Model

uncertainties are shown to be approximately 12 percent. Hyporheic water samples collected at the same depth as Temperature Javelins were analyzed using EPA method 800 on an Ion chromatograph to better understand solute transport in the discharging groundwater.

Chapter 5 Results

This chapter presents the Temperature Javelin and water quality sampling results for the Merced River flow path site. A brief assessment of the Temperature Javelin apparatus performance is instrumentation is presented, followed by analyses of vertical groundwater discharge velocities and water quality samples. Groundwater discharge temporal variation and spatial heterogeneity are discussed and possible flow induced nitrification zonation is hypothesized.

5.1 iButton Performance and Limitations

Thermocron iButtons are not designed to be submersible despite with mixed reviews in the literature as to their water resistance (Johnson et al., 2005; Schmidt et al., 2007; Wolaver and Sharp, 2007), although Johnson's group reported only an 8% loss when deploying the iButtons to depths of up to 5 m over 12 months. In contrast, Wolaver (2007) reported lost 3 of 8 iButtons, a finding more consistent with the present work, when submersing them at depths of 2 to 6 m in freshwater for seven weeks (Wolaver and Sharp, 2007). Failure rates in excess of 60% were observed in this 3 month deployment. The use of iButtons to monitor groundwater temperature has been well documented (Johnson et al., 2005; Schmidt et al., 2007). Upon retrieval of the iButtons, only 19 out of the 45 iButtons were able to be downloaded. Fortunately, data were recovered from at least one iButton at all but one javelin location, therefore sufficient data were amiable to provide results of groundwater surface water interactions. Further communications with Dallas Semiconductors has confirmed that there is variability in manufacturing process with respect to the seal on the iButton. It is believed that not only the depth and subsequent pressure cause the iButtons to fail, but also the duration that the iButton is submerged.

As a result of the excessive failure rates, an investigation of methods to improve the lifetime of iButtons while submerged is underway. A waterproof "capsule" for the iButton (Model DS9107) is now available, but this significantly changes the size of the overall sensor (35 x 25 mm versus 17.3 x 6 mm). Fortunately, it appears to be the case that simply coating the iButton casing with epoxy or other waterproof agents may render them sufficiently robust to long-term deployments at significant depths in the water column (Hatch, 2009). Discussion on the potential use of Thermocron iButtons for measuring gw-sw interactions is continued in Chapter 6.

5.2 Temperature Results

Flows between October 2008 and January 2009 ranged from 7.8m^3/s (203ft^3/s) to 12.2m^3/s (432ft^3/s) with a median value of 8.3m^3/s (291ft^3/s), although associated stage changes for this reach were modest, ranging from about 17.4 to 17.7 m over the same timeframe. Because a steady pressure differential is assumed in equation (9), stage changes of this magnitude bias interpreted discharge rates, particularly during the times when discharges are relatively low. Over the time of this study, the surface water temperature decreased from approximately 16˚C to about 8˚C and groundwater temperature, measured 20 m below ground surface, remained nearly constant at 19.5˚C (**Figure 5.1**). The decrease in surface water temperature during this period enhances the difference between the groundwater and surface water temperatures. In doing so, it reduces the uncertainty of the analytical model derived from the temperature difference is reduced (**Figure 5.2**). The maximum temperature difference

achieved in the winter (approximately 11.5˚ C here) reduces the relative error in estimated local gw-sw discharge rates to less than 2%.

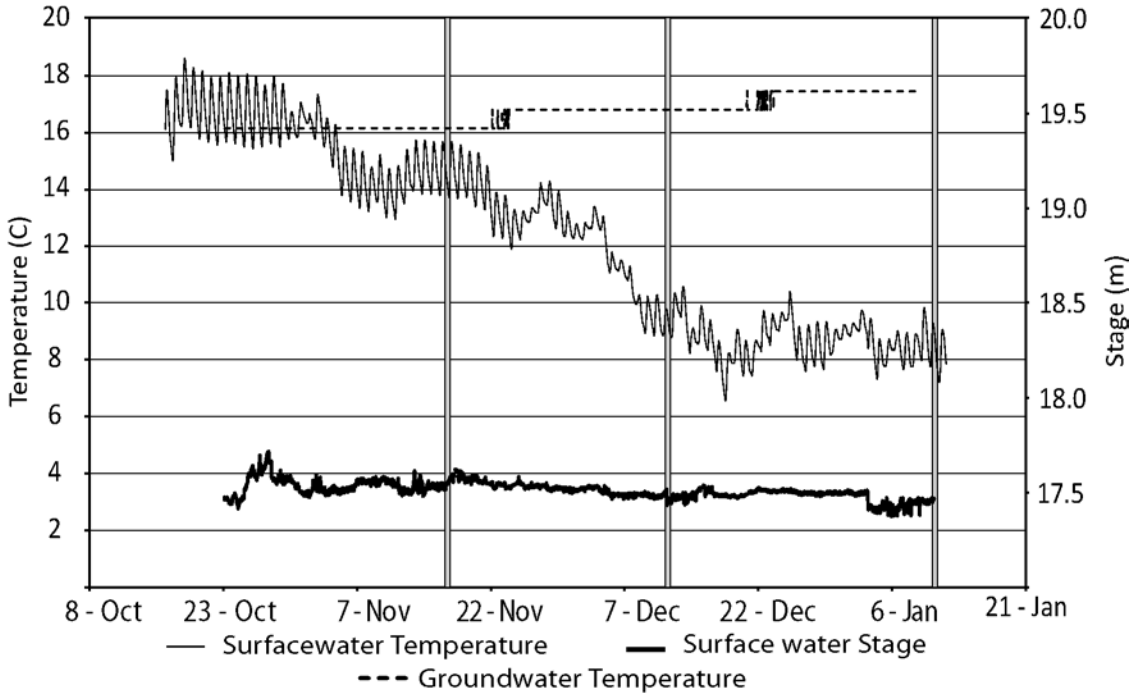

Figure 5.1 – Groundwater, surface water stage and temperature with water sampling events shaded.

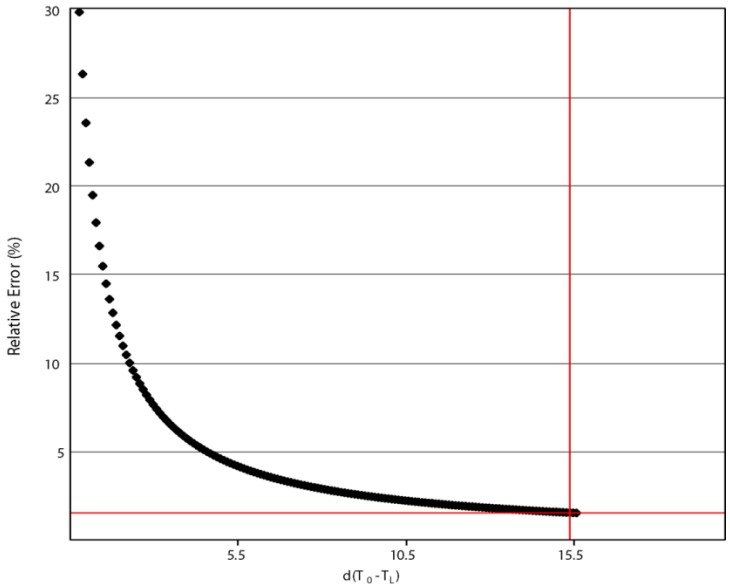

Figure 5.2 - Surface water decreasing relative error in estimated gw-sw discharge rate as a function of gw-sw temperature difference.

Surface water temperature data are highly variable both diurnally and seasonally through the first part of December (**Figure 5.1**). Riverbed temperatures cool at similar rates throughout the experiment regardless of depth. The observations in this work are consistent with those of previous investigations, with temperatures nearest to the groundwater source being relatively warmer surface water (**Figure 5.3**, **Figure 5.4**) (Domagalski et al., 2007; Essaid et al., 2008; Zamora, 2007). By December, surface water flows and temperatures begin

to stabilize toward steady state conditions (**Figure 5.1**), as do the riverbed temperatures by the first part of January (**Figure 5.3**).

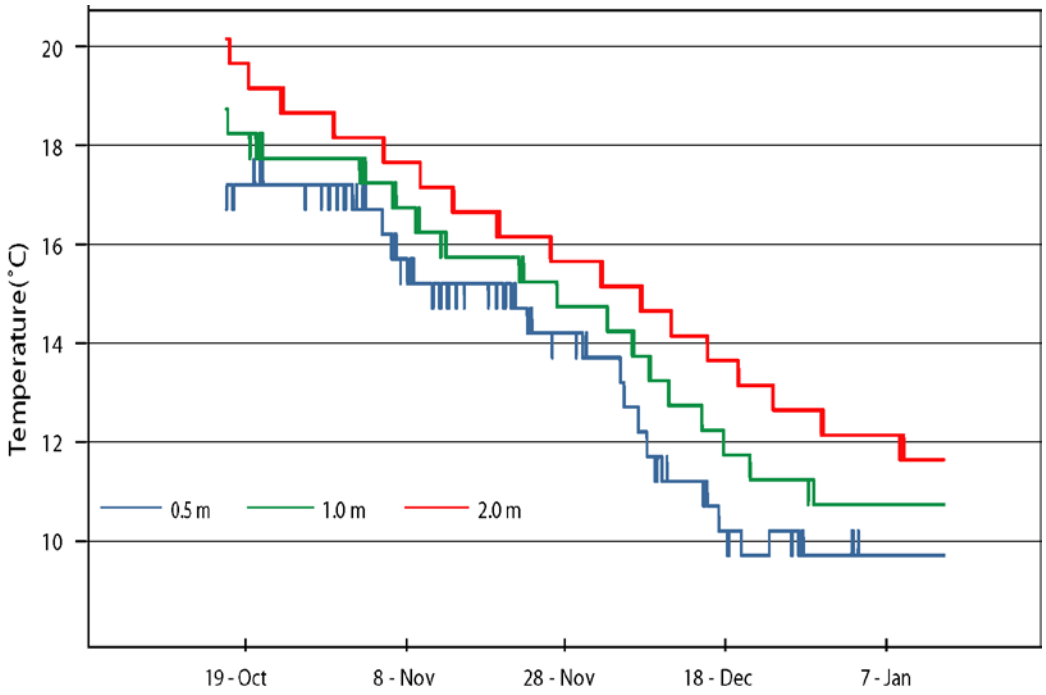

Figure 5.3 - Javelin 8 temperature profiles at depth demonstrating a consistent cooling trend Oct-Dec, followed by more stationary conditions in January.

5.3 Velocity Results

Vertical groundwater discharge velocities were calculated using the Turcotte and Schubert (1982) analytical method (see Ch 4, equation 9), and assume quasi-steady state conditions at any moment in time. More specifically this assumes that the changes in temperature and stage are sufficiently slow to allow the steady state assumption to be employed using the observed temperature gradients. Velocity estimates are plotted at 3 different depths from Javelin 8 in **Figure 5.4**. Variable river flows are apparent throughout the deployment, though stage changes only minimally (17.3 m to 17.5 m, see **Figure 5.1**), with longer-term quasi-steady state flow conditions beginning in the early part of December. Groundwater discharge velocities show similar patterns in variability throughout the deployment (**Figure 5.4**).

Diurnal cycling is evident in the surface water temperatures during throughout the fall due to the hot days and cool nights characteristic of this season. **Figure 5.4** shows the calculated vertical groundwater velocities using the Turcotte and Schubert analytical model. The first inset in **Figure 5.4** shows apparent diurnal cycling of the groundwater discharge velocities. This is a result of a relatively small temperature difference between the groundwater and surface water temperatures and the strong diurnal cycling of the surface water temperature. As noted by Schmidt et al. (2007), this degree of deviation from steady state conditions invalidates the discharge estimates made using the approach used here. Further

discussion of local temperature affects on calculated groundwater discharge velocities is continued at the end of this section.

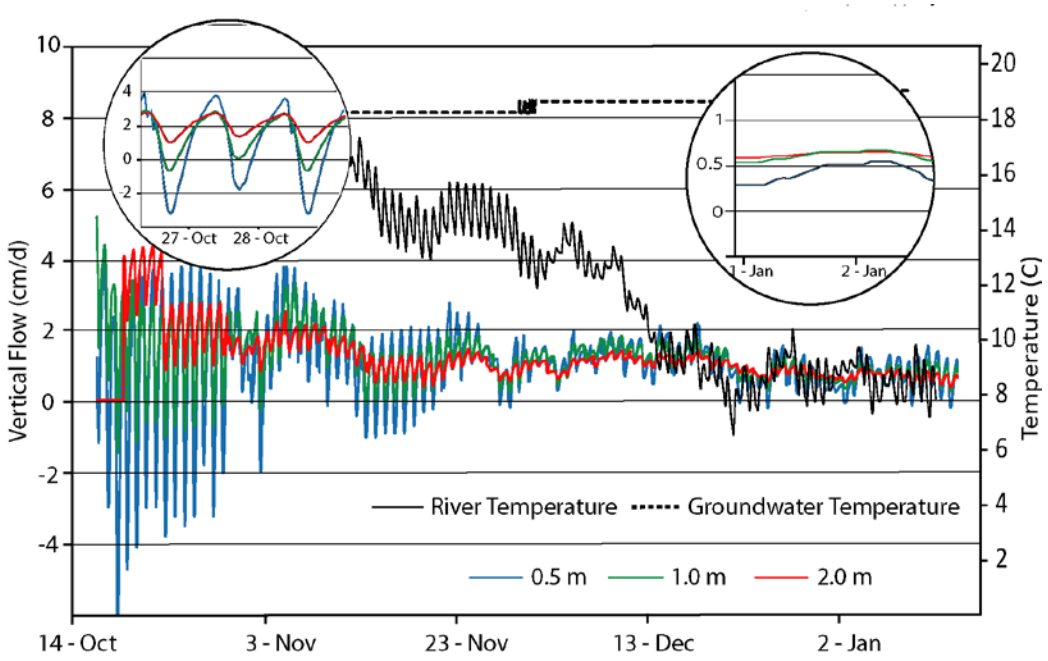

Figure 5.4 - Estimated vertical gw-sw discharge velocities at temperature observation depths indicated (black line indicates river discharge rate).

The second inset in **Figure 5.4** characterizes relatively lower and more stable flows, along with less prominent diurnal variation in estimated groundwater discharge velocities. Apparent diurnal cycling is evident, but over a smaller range. Velocities for these lower flow conditions are observed to approach similar values regardless of the depth in the riverbed. Riverbed temperatures at this time have stabilized at their annual minima. Constantz and Thomas (1997) observed diurnal discharge cycles tied to surface water temperature cycling (Constantz and Thomas, 1997).

A spatial mapping of the calculated gw-sw discharges for the two transects taken at each sampling period is shown in **Figure 5.5**, (downstream-looking convention) with velocity increasing as circles pass from blue to red. Overlapping measurements are measurements along the same line of action within a single transect. Velocities in **Figure 5.5** are averaged over a ten day period centered on the date of the water sampling event. Despite differences in averaged vertical groundwater velocities (0.1 to 6.8 cm/day) in **Figure 5.5**, both transects show similar velocity profiles with slightly higher velocities on the right (north) side. Thus, groundwater inputs are shown to be greater from the right side of the river along this reach. The lowest velocities were found in the upstream transect on the left side of the river near a pool with a fallen tree upstream reducing the flow in the pool. Consistently higher values (0.6 to 2.9 cm/day) are shown near the pool in the lower transect. The highest velocities (4.2 to 6.8 cm/day) are found closer to the right side of the river (**Figure 5.5**).

The upstream transect is free from all obvious debris in the riverbed with the exception to a fallen tree on the left bank extending into the pool where the left most Javelin in the upstream transect is located. In contrast the downstream transect is littered with multiple

October and December groundwater discharge vertical velocity calculations are generally higher than those in January. It should be noted, however, that the velocities calculated from the October temperature gradients have the largest uncertainty due to the more modest groundwater and surface water temperature differences and transient conditions noted above (**Figure 5.1**). As the surface water streambed temperature begins to reach "steady-state" conditions and the difference between surface water and groundwater temperature is greatest, the discharge values become more stable (**Figure 5.4**). As a result, January discharge velocities tend to be much more homogeneous and at a lower average rate with the exception of the right side of the upstream transect (**Figure 5.5**).

Results show there is inconsistency between groundwater discharge velocities near the center left of the downstream transect in the same line of action only 4 meters up/downstream. This may to be caused by hyporheic pumping caused by submerged obstacles (stumps) upstream of the relevant Temperature Javelin. As water passes around the stump, water is forced into the riverbed. The water passing over the stump creates a localized pressure drop and water is drawn up or "pumped" from the hyporheic back into the water column (Elliott and Brooks, 1997) (see **Figure 3.2**). This pumping action could cause increased velocity readings to be observed. It is unknown to what spatial extent a submerged object could affect the surrounding gw-sw interactions. Additional work is needed to determine the velocity field around such semi-submersed obstructions. Zamora (2008) and Essaid (2008) show similar results, where variable rates of discharge and recharge are found in the riverbed substrate.

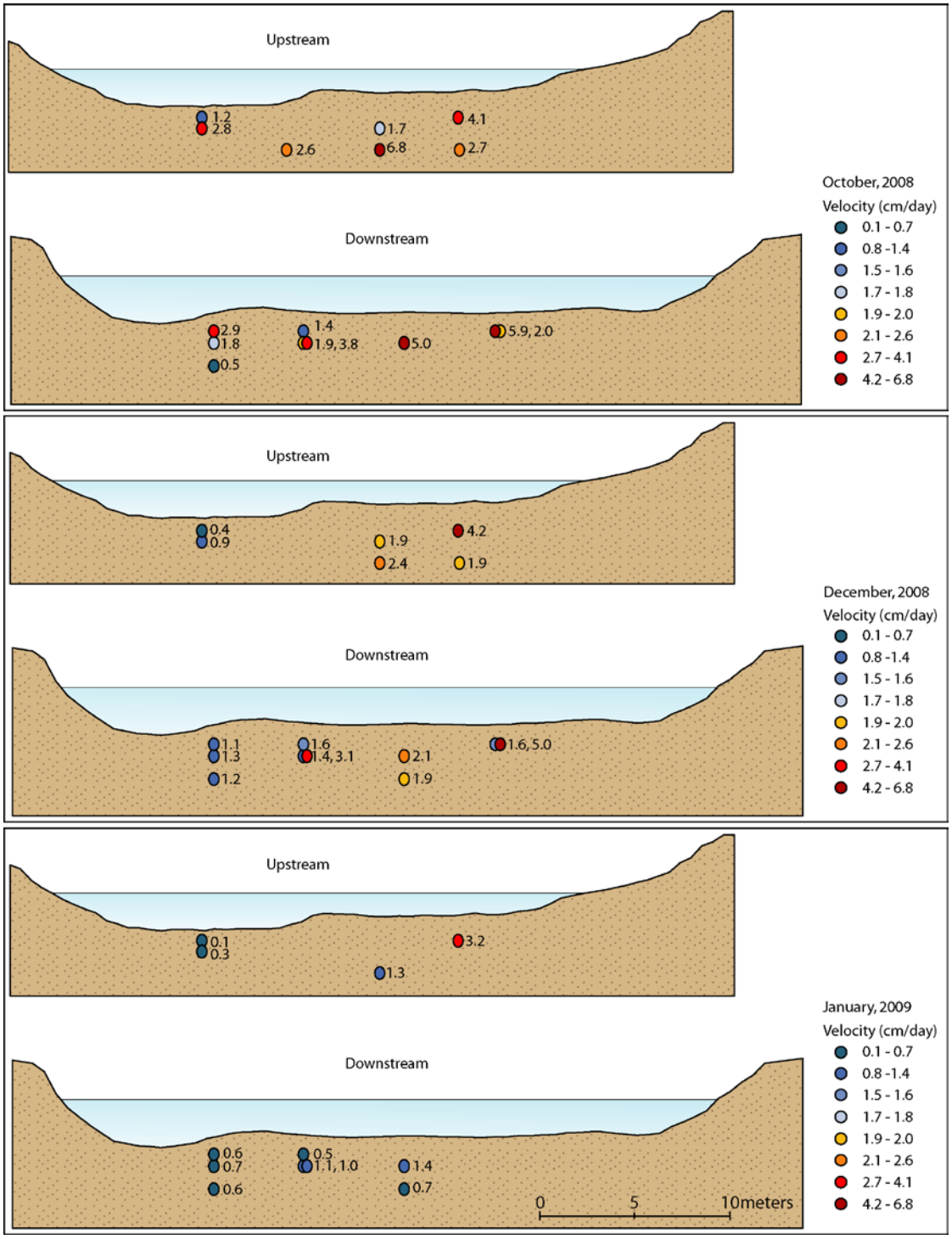

Figure 5.5 – Velocity profiles averaged over ten days about water sampling dates of the upper and lower transects looking downstream.

5.4 Water Quality Sampling Results

Groundwater, riparian, and hyporheic water samples provide evidence for mixing, plant uptake, and biogeochemical transformations. Solute concentrations support previous conclusions that surface water mixing extends below 1m into the streambed. Nitrate and ammonium concentrations are heterogeneously distributed throughout the subsurface. Riparian plant and macrophyte uptake is possibly given in ammonium sampling results. Finally, flow induced nitrification is hypothesized from groundwater discharge velocities and hyporheic water samples.

5.4.1 Surface Water Mixing

Pucket et al. (2008) reported that surface water mixing is evident at this study site up to depths of 1 m in the hyporheic zone, and not withstanding diurnal fluctuations in the surface water, this is not seen definitively in the temperature data. However, the water quality data suggests that this may be the case. Both nitrate and ammonium concentrations were shown to be distributed relatively homogeneously at shallower riverbed depths. Nitrate and ammonium concentrations in the river and shallow depths were observed between 2.1 to 50 parts per million (ppm), and 0.06 to 0.12 ppm, respectively with no differentiation of solute composition with depth.

5.4.2 Nitrate Results

Observed nitrate concentrations ranged from 0 to 50 ppm in the upstream transect and 0 to 52 ppm in the downstream transect whereas, as noted above, nitrate concentrations in the surface water range between 2 and 3 ppm (**Figure 5.6**). The upstream transect exhibited larger values (in excess of 39 ppm) in the right riparian wells at multiple depths in each sampling set. Downstream transect sampling revealed relatively lower values along most of the transect, with maximum observed values of about 52 ppm. Pucket et al. (2008) found similar results with elevated values at the right side of the upstream transect and the center left of the downstream transect was for the center left of the downstream transect (Puckett et al., 2008).

The highest observed nitrate concentrations in the riparian wells (30 to 52 ppm) are in the range of goundwater concentrations (12 to 76 ppm) on the right side of the river. It is believed that groundwater in the riparian zone has undergone only minor nitrogen uptake by plants, dentrification and/or mixing in the hyproheic zone. Downstream concentrations in the middle-left of the transect increase with time as do the right side of the upstream transect.

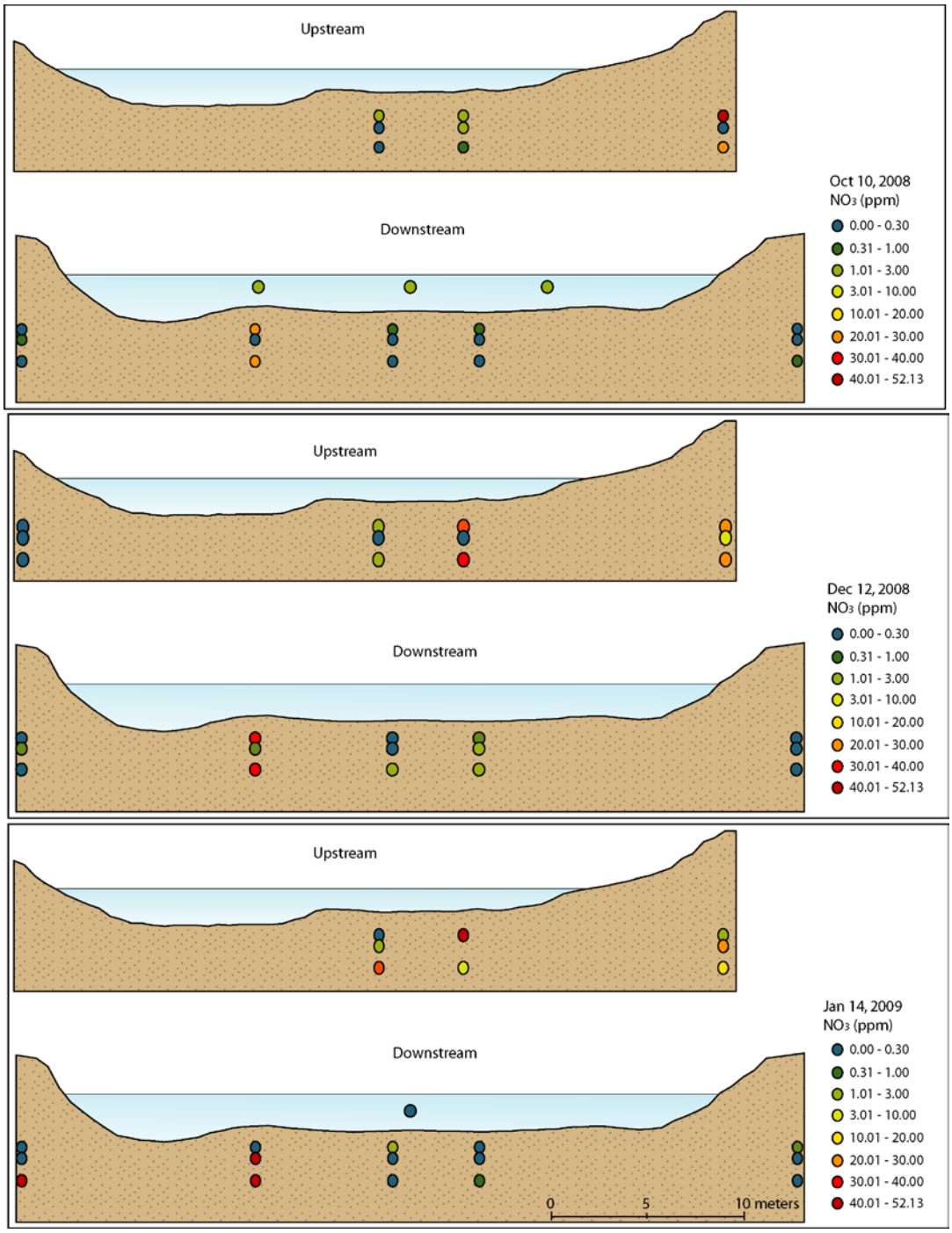

Figure 5.6 - Nitrate concentration profiles showing upper transect above the lower transect, looking downstream

5.4.3 Ammonium Results

Ammonium concentrations in the surface water and hyporheic zone were minimal, ranging from trace (~0.01) to 2 ppm (**Figure 5.7**). In addition, all groundwater samples were found to have non-detectable ammonium levels, suggesting that some denitrification of nitrate is taking place along the gw-sw flow path. The maximum ammonium concentrations observed

(0.6 to 2 ppm) were along the left side of the downstream transect. Ammonium concentrations appeared to decrease in the upper transect over the fall to winter season, but the values were all low sufficiently low to suggest that mixing of the surface water may have caused these detections.

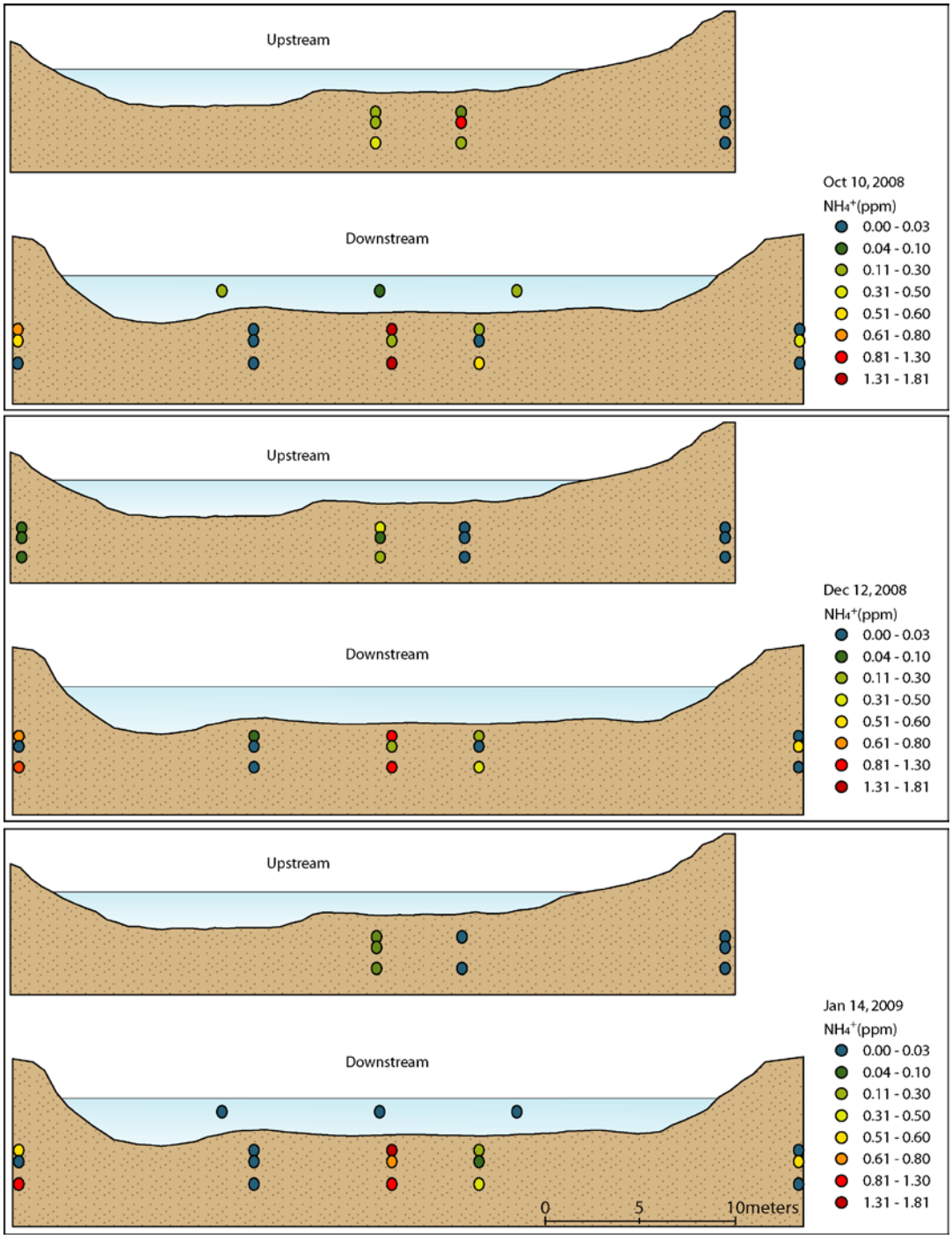

Figure 5.7 - Ammonium concentration profiles showing upper transect above the lower transect, looking downstream.

5.4.4 Plant Uptake

Biogeochemical transformations were not directly assessed but were inferred the solute constituents observed at various locations. Without any chemical transformation riparian and hyporheic waters should have the same composition as groundwater before the discharging groundwater mixes with the surface water. However, we see that riparian and hyporheic nitrate concentrations are much lower than groundwater samples and ammonium concentrations are evident in many of the hyporheic and riparian water samples (**Figure 5.6**, **Figure 5.7**).

There is an abundant expanse of riparian vegetation along the right side of the river, whereas there is only a narrow strip along the left side of the river at the upstream transect and no riparian vegetation along the left side of the river at the downstream transect. The large expanse of riparian vegetation and macrophytes on the right side of the river is capable of removing ammonium and nitrate (in right side of the downstream transect). The absence of a riparian strip along the left side of the downstream transect correlates with higher ammonium concentrations (**Figure 5.7**).

5.4.5 Flow Induced Nitrification Cycling

Downstream concentrations of ammonium were slightly higher than the upstream, with small patches of elevated ammonium bounded by areas of relatively high nitrate and corresponding increased groundwater discharge (**Figure 5.5**, **Figure 5.6**, **Figure 5.7**). Patrick and Ready (1976) describe a mechanism of ammonium nitrifying to nitrate, with the presence of aerobic areas in the riverbed adjacent to anaerobic areas. Patrick and Ready (1976) described oxygenated water entering the streambed and penetrating to a certain depth, and establishing an aerobic layer with an anaerobic layer below cutoff from the oxygenated surface water. Ammonium is nitrified in the aerobic layer, and excess nitrate is denitrified in the anaerobic layer. A diffusional gradient develops between the two layers, where produced nitrate diffuses into the anaerobic layer and ammonium diffuses from the anaerobic to the aerobic layer (Patrick and Reddy, 1976).

It is hypothesized that at this location, the heterogeneous groundwater discharges create nitrification cells rather than horizontal layers propagated from groundwater discharge in combination with surface water mixing in the hyporheic zone. Preferential flow paths allow nitrate rich groundwater to discharge into the river at varying rates. This heterogeneity permits ammonium enriched surface water to penetrate deeper into the substrate at areas of lower discharge creating aerobic zones sustained by the oxygenated surface water and bounded by higher groundwater discharge flow paths. Ammonium is nitrified in the aerobic zone into nitrate and the resultant nitrate is transported into the water column via hyporheic mixing or groundwater discharge. (**Figure 5.8**)

Vertical groundwater discharge velocities are found where hyporheic nitrate concentrations are highest and adjacent to elevated ammonium zones (**Figure 5.5**). In this case, nitrate rich groundwater infiltrates the hyporheic zone along flow paths within greater hydraulic conductivity adjacent to areas of lower hydraulic conductivity. Surface water is able to mix to depths in excess of 2 m in this stretch of the Merced River and may transport ammonium to these. There were no dissolved oxygen (DO) measurements taken during this investigation, so it

is unknown whether the areas of differing groundwater discharge are in fact aerobic, and/or anaerobic.

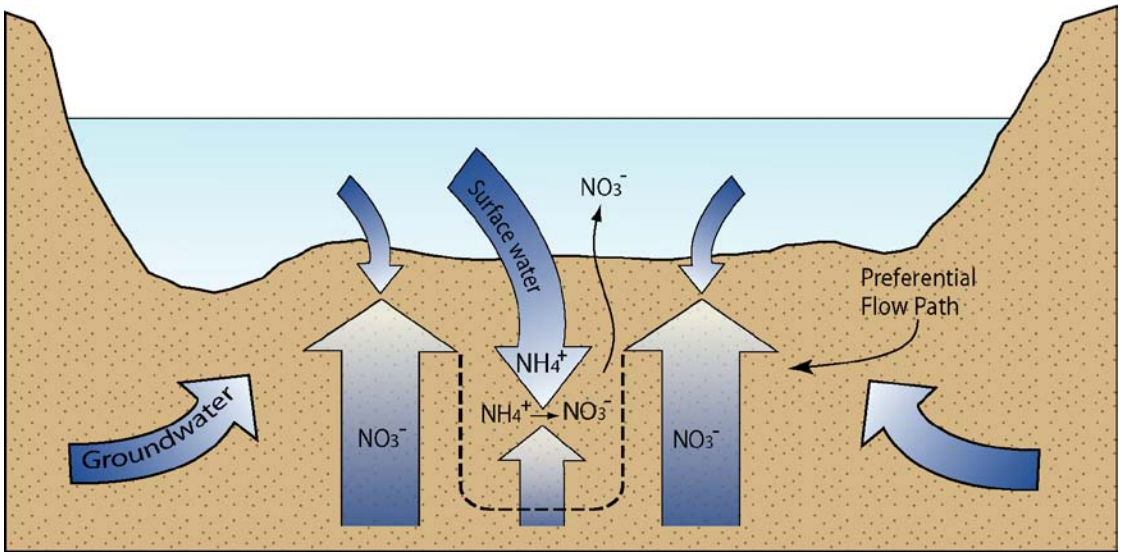

Figure 5.8 – Idealized conceptual model for flow induced denitrification cell development in the hyporheic zone (after (Patrick and Reddy, 1976)).

Temperature Javelins calculations and water quality samples provide a greater detailed understanding of hyporheic processes at this location than were previously presented. Vertical groundwater discharge velocities are shown to be within agreement with previously carried out investigations. Water quality samples taken from hyporheic drive points provide insight into biogeochemical reactions such as the possible presence of flow-induced nitrification cells, or other biogeochemical features and processes supporting the observed patterns in gw-sw discharge and N species.

Chapter 6 Conclusions and Future Work

6.1 Conclusions

Temperature Javelins make improvements over other methods for calculating groundwater discharge. Despite the setbacks with the use of unmodified Thermocron iButtons, they show great potential for increased deployment longevity after simple modifications. Vertical groundwater discharge velocities show similar results to previous investigations. Finally, flow induced nitrification cells are hypothesized to from the conjunctive use of groundwater velocity calculations and hyporheic water samples.

Specific outcomes from this work are as follows:

- Temperature Javelins improve upon many of the limitations of current gw-sw or hyporheic exchange monitoring devices through their speed of deployment in many river systems and a low equipment costs. Temperature Javelins reduce material costs through the use of readily available components, and significantly reduce deployment times to below 10 minutes per Javelin. These two attributes allow for rapid and larger spatial investigations to be attainable using a smaller amount of resources, which is capable of meeting the data demands of three-dimensional models which are not typically used due to the lack of sufficient data.
- Despite their failure rate, Thermocron iButtons have the potential to be extremely useful for environmental monitoring, if properly waterproofed, due to their size and ease of use. Preliminary investigations have shown that iButtons were water tolerant for shorter deployments on the order of 2 to 3 weeks.
- The Turcotte and Schubert (1982) analytical one-dimensional vertical groundwater discharge model produces reliable estimates of groundwater discharge velocities provided that there is a sufficient difference (approximately 2 °C) between groundwater and surface water temperatures. This model is only reliable where the streambed temperature is greater than the surface water temperature and less than or equal to the groundwater temperature (gaining river conditions).
- At the site of this investigation, nitrate and ammonium concentrations were observed to be heterogeneous in both transects due to hyporheic mixing of surface and groundwater, plant uptake and biogeochemical transformations. Determining the dominant processes is difficult, and future work is needed in this area at this site. Preferential flow paths appear to be conducting nitrate rich groundwater to discharge into the river at varying rates. Spatially heterogeneity of the flow field (possibly due to hydraulic conductivity variation) also appears to permit surface water to penetrate deeper into the substrate in areas of lower discharge, and creating isolated anaerobic zones bounded by the oxygenated surface water. These flow-induced nitrification cells are hypothesized to be present as a sink for hyporheic ammonium.

6.2 Future Directions

The use of heat as a tracer to monitor groundwater flow is a useful and easy-to-implement strategy. Furthermore, Temperature Javelins enable the user to monitor gw-sw interactions at an extremely low cost and are deployable with little effort in alluvial stream deposits, provided

the substrate texture does not exceed that of coarse sand. To identify the origin of groundwater, the chemical composition must be known along a flow line. The pairing of temperature and chemical monitoring is therefore requisite for this application. To meet this requirement, sampling tubing is planned to be incorporated into the Temperature Javelin to provide samples at corresponding depths to the temperature measurements. This integration will allow the user to access the necessary information to monitor groundwater into a single tool that is easily deployed as well as both cost and labor effective (**Figure 6.1**).

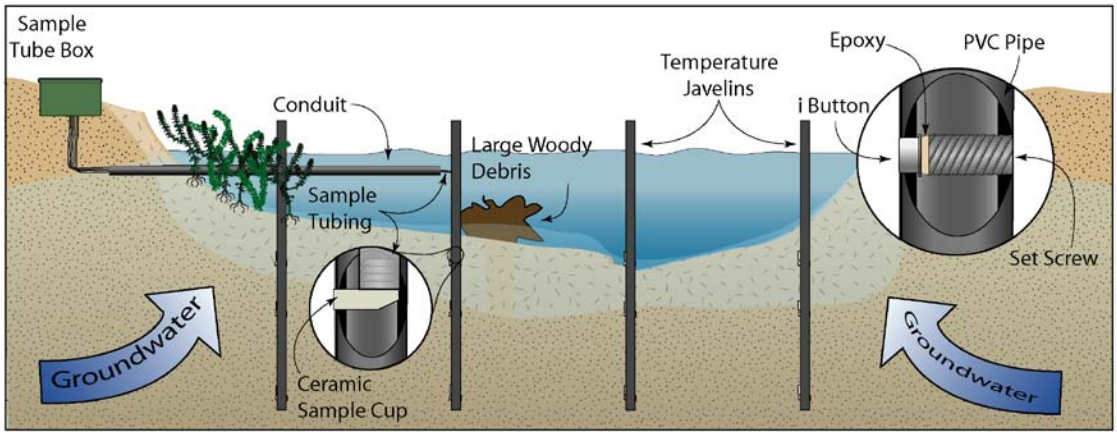

Figure 6.1 - Temperature Javelin with integrated water sample cups and tubing

Agricultural land use adjacent to rivers is known to be a contributor to the declining health of these rivers. As a non-point source of pollution, understanding of sustainable land use practices are unknown. Hence, understanding the connection between land management practices and non-point source pollution, as it is associated with gw-sw discharges in agricultural settings is critical. The preceding method when paired with groundwater samples is able to connect the endpoints of this “non-point source” pollution. Isotopic analysis of these water samples may enable determining the origin of the nutrient loads and other chemical constituents within the groundwater moving towards the river. Future development and use of this method are needed to shed light on the origin of non-point source pollution and to help formulate sustainable management decisions on sustainable agricultural land near surface water.

Chapter 7 References

Anderson, M.P., 2005. Heat as a Ground Water Tracer. Ground Water, 43(6): 951-968-951-968.

Bencala, K.E., 1993. A Perspective on Stream-Catchment Connections. Journal of the North American Benthological Society, 12(1): 44-47.

Bencala, K.E., 2000. Hyporheic zone hydrological processes. Hydrological Processes, 14(15): 2797-2798.

Bencala, K.E., 2005. Hyporheic Exchange Flows, Encyclopedia of Hydrological Sciences. John Wiley and Sons, New Jersey, pp. 1,733-1,740.

Bevington, P.R. and Robinson, D.K., 1992. Data reduction and error analysis for the physical sciences. McGraw-Hill, New York, 328 pp.

Birgand, F., Skaggs, R.W., Chescheir, G.M. and Gilliam, J.W., 2007. Nitrogen removal in streams of agricultural catchments - A literature review. Critical Reviews in Environmental Science and Technology, 37(5): 381-487.

Bredehoeft, J.D. and Papadopulos, I.S., 1965. Rates of vertical groundwater movement estimated from the Earth's thermal profile. Water resources research, 1(2): 325.

Burow, K.R., Shelton, J.L., Hevesi, J.A. and Weissmann, G.S., 2004. Hydrologic Characterization of the Modesto Area, San Joaquin Valley California. 2004-5232, U.S. Geological Survey.

Capel, P.D., McCarthy, K.A. and Barbash, J.E., 2008. National, Holistic, Watershed-Scale Approach to Understand the Sources, Transport, and Fate of Agricultural Chemicals. Journal of Environmental Quality, 37(3): 983-993.

Cardenas, M.B. and Zlotnik, V.A., 2003. Three-dimensional model of modern channel bend deposits. Water Resources Research, 39(6): -.

Chambers, P.A., Prepas, E.E., Bothwell, M.L. and Hamilton, H.R., 1989. Roots Versus Shoots in Nutrient-Uptake by Aquatic Macrophytes in Flowing Waters. Canadian Journal of Fisheries and Aquatic Sciences, 46(3): 435-439.

Conant, B., 2004. Delineating and quantifying ground water discharge zones using streambed temperatures. Ground Water, 42(2): 243-257.

Constantz, J., 1998. Interaction between stream temperature, streamflow, and groundwater exchanges in alpine streams. Water Resources Research, 34(7): 1609-1616.

Constantz, J., Stonestrom, D., Stewart, A.E., Niswonger, R.G. and Smith, T.R., 2001. Analysis of streambed temperatures in ephemeral channels to determine streamflow frequency and duration. Water Resources Research, 37(2): 317.

Constantz, J. and Thomas, C.L., 1997. Streambed temperatures profiles as indicators of percolation characteristics beneath arroyos in the Middle Rio Grande Basin, USA. Hydrological Processes, 11(12): 1621.

Constantz, J., Thomas, C.L. and Zelleger, G., 1994. Influence of diurnal variations in stream temperature on streamflow loss and groundwater reacharge. Water Resources Research, 30(12): 3253-3264.

Cooper, A.B. and Cooke, J.G., 1984. Nitrate Loss and Transformation in 2 Vegetated Headwater Streams. New Zealand Journal of Marine and Freshwater Research, 18(4): 441-450.

Domagalski, J.L. et al., 2008. Comparative Study of Transport Processes of Nitrogen, Phosphorus, and Herbicides to Streams in Five Agricultural Basins, USA. Journal of Environmental Quality, 37(3): 1158-1169.

Domagalski, J.L. et al., 2007. Influences of the unsaturated, saturated, and riparian zones on the transport of nitrate near the Merced River, California, USA. Hydrogeology journal.

Domenico, P.A. and Schwartz, F.W., 1990. Physical and chemical hydrogeology. Wiley, New York.

Elliott, A.H. and Brooks, N.H., 1997. Transfer of nonsorbing solutes to a streambed with bed forms: Laboratory experiments. Water Resources Research, 33(1): 137-151.

Essaid, H.I., Zamora, C.M., McCarthy, K.A., Vogel, J.R. and Wilson, J.T., 2008. Using Heat to Characterize Streambed Water Flux Variability in Four Stream Reaches. Journal of Environmental Quality, 37(3): 1010-1023.

Fisher, L.H. and Healy, R.W., 2008. Water Movement within the Unsaturated Zone in Four Agricultural Areas of the United States. Journal of Environmental Quality, 37(3): 1051-1063.

Green, C.T., Fisher, L.H. and Bekins, B.A., 2008a. Nitrogen Fluxes through Unsaturated Zones in Five Agricultural Settings across the United States. Journal of Environmental Quality, 37(3): 1073-1085.

Green, C.T. et al., 2008b. Limited Occurrence of Denitrification in Four Shallow Aquifers in Agricultural Areas of the United States. Journal of Environmental Quality, 37(3): 983-983-993.

Gronberg, J.M. and Kratzer, C.R., 2006. Environmental Setting of the Lower Merced River Basin, California. 2006-5152, U.S. Department fo the Interior; U.S. Geological Survey.

Hancock, T.C. et al., 2008. Pesticide Fate and Transport throughout Unsaturated Zones in Five Agricultural Settings, USA. Journal of Environmental Quality, 37(3): 1086-1100.

Hatch, C., University of Nevada-Reno, 2009. In: T. Harmon, C. (Editor).

Johnson, A.N. et al., 2005. Evaluation of an Inexpensive Small-Diameter Temperature Logger for Documenting Ground Water-River Interactions. Ground water monitoring remediation, 25(4): 68.

Lapham, W.W., 1989. Use of Temperature Profiles Beneath Streams to Determine Rates of Vertical Ground-Water Flow and Vertical Hydraulic Conductivity. Water Supply Paper 2337, U.S. Geological Survey.

Nielsen, L.P. and Sloth, N.P., 1994. Denitrification, nitrification and nitrogen assimilation in photosynthetic mats. NATO ASI Series G Ecological Sciences, 35.

Patrick, W.H. and Reddy, K.R., 1976. Nitrification-Denitrification Reactions in Flooded Soils and Water Bottoms - Dependence on Oxygen-Supply and Ammonium Diffusion. Journal of Environmental Quality, 5(4): 469-472.

Phillips, S.P., Green, C.T., Burow, K.R., Shelton, J.L. and Rewis, D.L., 2007. Simulation of Multiscale Ground-Water flow in Part of the Northeastern San Joaquin Valley, California. 2007-5009, U.S. Geological Survey.

Puckett, L.J. et al., 2008. Transport and Fate of Nitrate at the Ground-Water/Surface-Water Interface. Journal of Environmental Quality, 37(3): 1034-1050.

Ronan, A.D., Prudic, D.E., Thodal, C.E. and Constantz, J., 1998. Field study and simulation of diurnal temperature effects on infiltration and variably saturated flow beneath an ephemeral stream. Water Resources Research, 34(9): 2137-2153.

Rorabaugh, M.I., 1956. Groundwater in northeastern Louisville Kentucky with reference to induced infiltraion. 1360-B, U.S. Geological Survey, Washington, D.C.

Salehin, M., Packman, A.I. and Paradis, M., 2004. Hyporheic exchange with heterogeneous streambeds: Laboratory experiments and modeling. Water Resources Research, 40(11): -.

Schmidt, C., Conant, B., Bayer-Raich, M. and Schirmer, M., 2007. Evaluation and field-scale application of an analytical method to quantify groundwater discharge using mapped streambed temperatures. Journal of Hydrology, 347(3-4): 292-307.

Slichter, C.S., 1905. Field Measurements of the Rate of Movement of Underground Waters, Water-Supply and Irrigation Paper No. 140. U.S. Geological Survey, Washington, DC.

Stallman, R.W., 1963. Computation of Ground-water Velocity From Temperature Data. In: Anonymous (Editor), Methods of collecting and interpreting ground-water data. U.S. Geological Survey, pp. H36.

Stallman, R.W., 1965. Steady one-dimensional fluid flow in a semi-infinite porous medium with sinusoidal surface temperature. Journal of geophysical research, 70(12): 2821.

Steele, G.V., Johnson, H.M., Sandstrom, M.W., Capel, P.D. and Barbash, J.E., 2008. Occurrence and Fate of Pesticides in Four Contrasting Agricultural Settings in the United States. Journal of Environmental Quality, 37(3): 1116-1132.

Stonestrom, D.A. and Constantz, J., 2003. Heat as a tool for studying the movement of ground water near streams, Circular 1260. U.S. Geological Survey.

Storey, R.G., Howard, K.W.F. and Williams, D.D., 2003. Factors controlling riffle-scale hyporheic exchange flows and their seasonal changes in a gaining stream: A three-dimensional groundwater flow model. Water Resources Research, 39(2): -.

Suzuki, S., 1960. Percolation Measurements Based on Heat Flow through Soil with Special Reference to Paddy Fields. Journal of geophysical research, 65(9): 2883-2883-2885.

Turcotte, D.L. and Schubert, G., 1982. Geodynamics applications of continuum physics to geological problems. John Wiley and Sons, Inc., New York, NY (US).

Vincent, W.F. and Downes, M.T., 1980. Variation in Nutrient Removal from a Stream by Watercress (Nasturtium-Officinale R Br). Aquatic Botany, 9(3): 221-235.

Vogel, J.R., Majewski, M.S. and Capel, P.D., 2008. Pesticides in Rain in Four Agricultural Watersheds in the United States. Journal of Environmental Quality, 37(3): 1101-1115.

Vogelmann, J.E. et al., 2001. Completion of the 1990s National Land Cover Data set for the conterminous United States from Landsat Thematic Mapper data and Ancillary data sources. Photogrammetric Engineering and Remote Sensing, 67(6): 650-+.

White, D.S., Elzinga, C.H. and Hendricks, S.P., 1987. Temperature Patterns within the Hyporheic Zone of a Northern Michigan River. Journal of the North American Benthological Society, 6(2): 85-91.

Winslow, J.D., 1962. Effect of stream infiltration on groundwater temperatures near Schenectady, N.Y. 450-C, U.S. Geological Survey, Washington, D.C.

Wolaver, B.D. and Sharp, J.M., 2007. Thermochron iButton: Limitation of this inexpensive and small-diameter temperature logger. Ground Water Monitoring and Remediation, 27(3): 127-128.

Zamora, C., 2007. Estimating Water Fluxes Across the Sediment-Water Interface in the Lower Merced River, California. 2007-5216, U.S. Geological Survey.

Chapter 8 Appendices

Appendix A. Water Sample Results

October 13, 2008 (10:00 am)

Distance	Elevatio	Depth	Transect	Na^+	NH_4^+	K^+	Mg^{2+}	Ca^{2+}	Cl^-	SO_4^{2-}	NO_3^-
12.53	14.3	1	T4	17.55	0	0.81	1.57	5.04	2.71	5.24	0
41.57	14.8	0.5	T4	29.96	0	1.69	9.08	19.62	9.99	3.98	0
12.53	14.8	0.5	T4	2.8	0	0.77	1.44	4.6	1.4	2.01	1.44
19.88	14.8	0.5	T4	21.09	1.52	1.63	5.91	21.36	7.31	0	0.03
19.88	14.3	1	T4	23.65	0.22	1.3	3.89	13.34	4.9	4.72	0
19.88	13.3	2	T4	18.88	1.79	1.66	5.91	25.6	6.34	0.14	0
12.53	13.3	2	T4	2.37	0.02	0.78	1.47	4.18	1.23	1.82	1.07
41.57	14.3	1	T2	43.02	0.5	2.14	9.59	20.37	11.01	51.36	0
41.57	13.3	2	T4	28.93	0	1.56	10.73	22.43	10.3	25.05	0.03
41	15.2	0.5	T2	39.57	0	1.97	14.55	35.37	13.12	54.26	35.43
26	15.2	0.5	T2	7.49	0.09	0.68	1.33	3.39	1.64	2.57	1.75
21.14	15.2	0.5	T2	2.91	0.25	0.92	1.76	5.21	1.47	1.93	1.2
21.14	14.7	1	T2	5.9	0.21	1.15	2.39	6.75	2.52	4.31	0.24
21.14	13.7	2	T2	2.57	0.34	0.87	1.61	5.76	1.2	1.05	0.15
26	14.7	1	T2	41.3	1.81	1.94	12.18	32.1	11.87	65.75	2.76
26	13.7	2	T2	3.65	0.18	0.55	1.82	3.98	1.43	2.64	0.93
41	14.7	1	T2	47.03	0	1.8	12.84	34.41	13.12	120.5	0.03
41	13.7	2	T2	37.28	0	1.96	14.27	35.46	12.98	54.12	28.8
0	13.3	2	T4	5.98	0	0.69	7.2	16.23	2.99	0	0
0	14.3	1	T4	34.83	0.52	0.82	3.56	6.87	6.76	0	0.02
0	14.8	0.5	T4	36.31	0.77	1	5.59	10.45	5.18	0	0
24.53	13.3	2	T4	3.61	0.56	0.86	3.47	14.56	1.92	0.71	0
24.53	14.8	0.5	T4	3.24	0.18	0.88	2.62	9.37	1.65	2.23	0.02
24.53	14.3	1	T4	11.71	0	0.98	2.05	6.87	3.27	4.54	0.01

December 12, 2008 (11:15 am)

Distance	Elevation	Depth	Transect	Na^+	NH_4^+	K^+	Mg^{2+}	Ca^{2+}	F^-	Cl^-	SO_4^{2-}	NO_3^-
41	15.2	0.5	T2	41.18	0	2.07	12.46	36.88	0.16	13.5	62.51	29.55
41	14.7	1	T2	49.21	0	1.91	10.88	35.56	0	12.66	107.5	6.57
41	13.7	2	T2	39.48	0	2.28	12.26	36.85	0	13.59	62.29	24.97
21.14	13.7	2	T2	3.43	0.12	0.79	0.72	2.73	0	2.52	3.22	1.5
21.14	15.2	0.5	T2	3.21	0.43	0.74	1.7	5.37	0	1.93	2.74	1.76
21.14	14.7	1	T2	3.25	0.1	0.78	1.88	4.73	0	2.3	5.94	0.43
26	15.2	0.5	T2	45.63	0	2.01	11.36	28.58	0	14.11	67.2	39.09
26	13.7	2	T2	31.58	0	1.77	11.29	24.64	0	13.67	57.66	40.13
12.53	14.8	0.5	T4	3.47	0.04	0.71	1.72	5.54	0.01	2.28	2.99	3.21
41.57	13.3	2	T4	34.77	0	1.86	12.53	30.94	0	12.61	72.48	0
41.57	14.3	1	T4	42.3	0.52	2.12	7.18	18.68	0.17	10.54	37.41	0
41.57	14.8	0.5	T4	35.01	0	2.05	9.32	24.65	0	11.72	49.16	0.03
19.88	14.8	0.5	T4	21.21	1.34	1.57	5.72	23.98	0.15	7.85	0.23	0
12.53	14.3	1	T4	18.52	0	1.18	3.48	12	0	4.83	11.31	0.03
12.53	13.3	2	T4	3.39	0	0.64	1.7	5.24	0	2.24	3.05	3.2
19.88	13.3	2	T4	15.38	1.14	1.46	5.13	25.3	0	5.46	0.09	0.05
19.88	14.3	1	T4	21.37	0.28	1.6	6.55	25.29	0.01	6.92	1.97	0
0	13.3	2	T4	29.2	0.84	1.11	5.98	12.98	0.73	2.6	0	0.01
0	14.3	1	T4	2.98	0	0.48	3.84	10.23	0.21	2.15	0.28	0.03
0	14.8	0.5	T4	35.89	0.62	0.87	3.22	6.99	1.01	3.65	0	0.01
24.53	13.3	2	T4	3.03	0.47	1.16	2.26	8.38	0	2.23	3.92	0.07
24.53	14.8	0.5	T4	2.57	0.26	0.51	2.07	10.99	0.1	2.07	1.13	0.03
24.53	14.3	1	T4	3.59	0	0.76	2.26	8	0.09	1.85	2.54	0.05
26	14.7	1	T2									
0	15.2	0.5	T2									
0	14.7	1	T2									
0	13.7	2	T2									
12.53	16	0	T4	3.85	0.12	0.7	1.64	5.95	0.08	2.62	3.06	2.45
19.88	16	0	T4	0.16	0.06	0.05	0.1	0.44	0.05	2.43	2.93	2.39
24.53	13.3	0	T4	3.59	0.11	0.66	1.56	5.44	0.05	2.52	2.98	2.31

January 14, 2009 (9:50 am)

Distance	Elevation	Depth	Transect	Na^+	NH_4^+	K^+	Mg^{2+}	Ca^{2+}	F^-	Cl^-	SO_4^{2-}	NO_3^-
41.57	14.8	0.5	T2	29.18	0	1.81	9.4	23.7	0.01	2.66	3.78	0.02
12.53	14.8	0.5	T2	4.06	0	0.6	2.26	6.4	0	11.35	51.1	0
19.88	14.8	0.5	T2	20.68	1.57	1.44	6.05	23.19	0.16	7.15	1.78	0.07
19.88	14.3	1	T2	21.6	0.63	1.56	7.86	27.63	0.18	12.83	69.87	0
19.88	13.3	2	T2	14.82	1.25	1.29	4.95	24.81	0.17	7.65	0	0
12.53	14.3	1	T2	39.39	0	1.79	9.82	33.54	0.02	3.29	4.47	3.53
12.53	13.3	2	T2	4.35	0	0.64	2.29	6.42	0.01	3.26	4.39	3.34
41.57	14.3	1	T2	42.31	0.6	2.07	7.52	18.44	0	10.53	22.62	0
41.57	13.3	2	T2	30.33	0	1.57	11.74	28.19	0.16	10.47	41.45	0
0	14.8	0.5	T2	31.72	0.57	0.75	3.17	6.17	0.7	2.41	0	0
24.53	14.8	0.5	T2	2.63	0.27	0.44	2.11	10.39	0.15	2.42	1	0.01
24.53	14.3	1	T2	3.34	0.04	0.72	2.88	9.11	0.1	2.42	1.22	0
24.53	13.3	2	T2	2.63	0.34	0.9	2.26	7.73	0.01	2.23	3.16	0.02
0	14.3	1	T2	2.82	0	0.38	4.09	9.77	0.96	2.93	0	0
0	13.3	2	T2	25.62	0.89	1.1	8.08	17.45	0.07	3.19	4.3	3.11
41	15.2	0.5	T4	40.01	0	1.95	12.92	35.82	0.06	3.34	4.5	2.49
26	15.2	0.5	T4	43.47	0	1.88	13.06	30.44	0.09	13.27	64.11	52.13
21.14	15.2	0.5	T4	4.31	0.1	0.67	2.22	6.13	0.05	2.5	6.28	0.23
21.14	14.7	1	T4	3.07	0.1	0.71	2.03	4.26	0.01	3.27	4.62	2.86
21.14	13.7	2	T4	4.39	0.08	0.78	1.96	5.03	0	13.37	72.66	39.27
26	13.7	2	T4	41.59	0	1.7	13.59	30.59	0.25	13.01	109.78	9.9
41	14.7	1	T4	47.95	0	1.79	10.59	34.37	0.09	13.45	64.47	20.12
41	13.7	2	T4	38.68	0	1.97	12.41	35.86	0.29	13.51	66.57	19.97